

RECENT RESULTS ON THE HADRONIC FINAL STATE IN
CHARGED CURRENT NEUTRINO AND ANTINEUTRINO REACTIONS

Norbert Schmitz

Max-Planck-Institut für Physik und Astrophysik
München, Germany

Introduction

Detailed experimental information on hadronic final states in neutrino induced reactions has been obtained so far, for obvious reasons (4π acceptance, measurement of individual tracks), only from bubble chambers. Recent contributions at high energies come from experiments, listed in Table 1, in the 15' chamber at Fermilab, in BEBC at CERN and in SKAT at Serpukhov. The first two chambers are equipped with external muon identifiers (EMI) to distinguish between charged-current (CC) and neutral-current (NC) events and to identify the muon in CC reactions. Various methods, based on transverse momentum balance¹⁻³, have been used to estimate the unmeasured incident neutrino energy E_ν . Earlier results on the hadronic final state as obtained with bubble chambers have already been published⁴⁻⁷.

The main features of the semi-inclusive reactions

$$\begin{aligned} \nu_\mu + N &\rightarrow \mu^- + h^\pm + X \\ \bar{\nu}_\mu + N &\rightarrow \mu^+ + h^\pm + X \end{aligned} \quad (1)$$

where h^\pm is a positive or negative hadron, are described by the naive quark-parton model (QPM) as sketched in Fig. 1. A quark in the nucleon absorbs the current (i.e. the intermediate boson W^\pm), thereby changes its flavor and fragments into the current fragments, whereas the remaining spectator quarks (di-quark) of the nucleon appear as target fragments. In contrast to electro- and muoproduction where several quark flavors contribute, the situation is particularly simple in $\nu(\bar{\nu})$ reactions: Neglecting the sea and the

Cabibbo angle it is the d (u) quark which absorbs the current to become a u (d) quark according to

$$\begin{aligned} \nu_\mu + d &\rightarrow \mu^- + u \\ \bar{\nu}_\mu + u &\rightarrow \mu^+ + d \end{aligned} \quad (2)$$

Thus the fragmentation functions $D_u^\pm(z)$ and $D_d^\pm(z)$ of the u and d quark into h^\pm can be studied in a rather clean way in ν and $\bar{\nu}$ reactions, respectively. The well known and frequently applied cascade model as developed, e.g. by Field and Feynman⁸ gives a quantitative description of the quark fragmentation process.

The variables describing the process of Fig. 1 are well known (four-momentum transfer q^2 , energy transfer ν in lab system, Bjorken-scaling variable x , effective mass of all

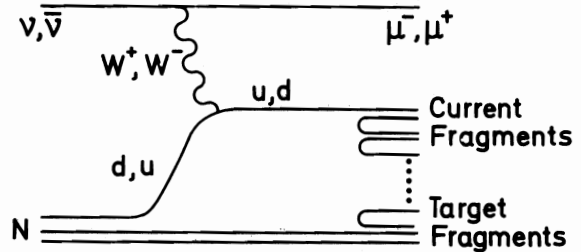


Fig. 1: Neutrino production $\nu/\bar{\nu}N + \mu^\mp + \text{hadrons}$ in the quark-parton model.

Table 1 Experiments from which results have been obtained recently

Bubble chamber, liquid	Beam	Number of CC events	Collaboration	Ref.
15' H ₂	$\bar{\nu}$ WBB	2250 $\bar{\nu}$, 500 ν	Argonne, Carnegie-Mellon, Purdue	15,50
15' Ne-H ₂	$\bar{\nu}$ WBB	7200 $\bar{\nu}$	Fermilab, IHEP, ITEP, Michigan	20
15' Ne-H ₂	$\nu, \bar{\nu}$ WBB	1200 ν , 1200 $\bar{\nu}$	Berkeley, Hawaii, Seattle	22
15' D ₂	ν WBB	660 ν	Illinois-Tech, Maryland, Sendai, Stony Brook, Tufts	23
BEBC Ne-H ₂	$\nu, \bar{\nu}$ NBB	1750 ν , 270 $\bar{\nu}$	Aachen, Bonn, CERN, London(I.C.), Oxford, Saclay	45,55
BEBC H ₂	ν WBB	5600 ν	Aachen, Bonn, CERN, München, Oxford	9,33,34,37
SKAT CF ₃ Br	ν WBB	417 ν	IHEP	24

final state hadrons $W =$ current-nucleon cms energy):

$$x = \frac{q^2}{2Mv} \quad \text{with } v = E_\nu - E_\mu, \quad y = \frac{\nu}{E_\nu} \quad (3a)$$

$$W^2 = M^2 + q^2 \left(\frac{1}{x} - 1 \right) \quad (3b)$$

For a final state hadron several longitudinal variables are used in the literature:

- energy fraction:

$$\left. \begin{aligned} z &= \frac{E^L}{E_H^L} = \frac{E^L}{\nu + M} \\ z' &= \frac{p \cdot h}{p \cdot q} = \frac{E^L}{\nu} \end{aligned} \right\} \Rightarrow z' = z \left(1 + \frac{2M^2 x}{q^2} \right) \quad (4)$$

$$z^* = \frac{2E^*}{W}$$

- momentum fraction:

in hadronic cms:

$$x_F = \frac{2p_{||}^*}{W} \quad (\text{Feynman } x) \quad (5a)$$

in Breit system⁺):

$$z_B = - \frac{2h \cdot q}{q^2} = \frac{2p_{||}^B}{q} \quad \text{or (in analogy to the Nachtmann variable)} \quad (5b)$$

$$\zeta = \frac{E^B + p_{||}^B}{q} = \frac{z_B}{2} \left(1 \pm \sqrt{1 + \frac{4m_T^2}{q^2 z_B^2}} \right)$$

for $z_B > 0$ (i.e. $\zeta > 0$) (ref. 8)

where $q \equiv \sqrt{q^2}$. At high energy $\frac{W}{2}$ ($\frac{q}{2}$) is the energy of the fragmenting quark in the cm system (Breit system).

- rapidity (e.g. in hadron cms):

$$y^* = \frac{1}{2} \ln \frac{E^* + p_{||}^*}{E^* - p_{||}^*} \quad (6)$$

Here the upper indices L, *, B refer to the lab, cm, Breit system respectively; p , q , h are the four-momenta of incident nucleon, current, final state hadron, respectively.

E_H^L is the lab energy of all outgoing hadrons and m_T the transverse mass given by $m_T^2 = m^2 + p_T^2$. For $q^2, W^2 \gg M^2$ the various quantities in (4) are nearly equal.

The two transverse variables of a final-state hadron are the momentum component \vec{p}_T transverse to the direction \vec{q} of the current (with components $p_{T \text{ in}}$ and $p_{T \text{ out}}$ in and perpen-

dicular to the lepton plane) and the azimuthal angle φ around the current direction with $\varphi = 0$ in the lepton plane, see Fig. 2.

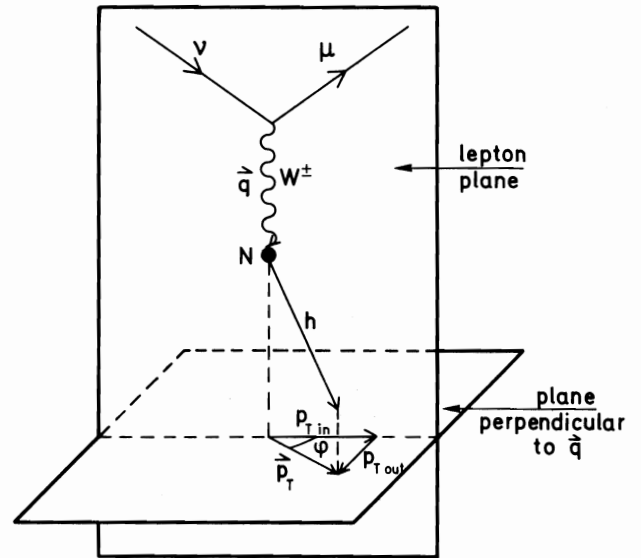


Fig. 2: Semi-inclusive neutrino production $\nu N + \mu + h +$ hadrons in the lab system: Definition of transverse momentum \vec{p}_T (with components $p_{T \text{ in}}$ and $p_{T \text{ out}}$) and azimuthal angle φ .

Much progress has been made lately in the analysis of the hadronic final state. According to the results obtained recently and submitted to this conference this rapporteur talk is subdivided into the following topics:

- A.) Multiplicities
- B.) Longitudinal properties of single hadrons
 - x_F and rapidity distributions
 - charge distributions, total net charges
 - fragmentation functions and their moments
- C.) Transverse properties of single hadrons
- D.) Jet studies

A.) Multiplicities

From previous experiments⁴⁻⁷ it is well known that the average multiplicity $\langle n \rangle$ of all charged hadrons in the inclusive reactions

$$\begin{aligned} \nu_\mu N + \mu^- + \text{hadrons} \quad (\text{i.e. } W^+ N \rightarrow \text{hadrons}) \\ \bar{\nu}_\mu N + \mu^+ + \text{hadrons} \quad (\text{i.e. } W^- N \rightarrow \text{hadrons}) \end{aligned} \quad (7)$$

is practically independent of q^2 at fixed W and that it increases linearly with $\ln W^2$.

New data on multiplicities for $W^2 \lesssim 150 \text{ GeV}^2$ come from the BEBC νH_2 collaboration⁹ based on ~ 5600 CC events. Fig. 3a shows the multiplicity distributions $P(n, W)$ vs W^2 with curves to guide the eye. The relative contributions from 2, 4 and 6 prongs are dropping

⁺The Breit system is the system in which the current has zero energy, i.e., momentum q . It has the velocity $1-2x$ in the cm system, i.e. it goes forward (backward) in the cms (with respect to the current direction) for $x < 0.5$ ($x > 0.5$)

at high W whereas those from higher prong numbers are still rising. Fig. 3b shows $\langle n \rangle$ vs W^2 together with a straight line fit of the form

$$\langle n \rangle = a + b \cdot \ln W^2 \quad (8)$$

Also shown are the straight line fits as obtained in other leptonproduction ($\bar{\nu}_p$ 4, e^-p 10, μ^-p 11) and in photoproduction 10,12 experiments, in the respective W ranges. The fitted values for a and b from the various experiments are compiled in Table 2. The $\bar{\nu}_p$ multiplicity is lower than the ν_p multiplicity, but has roughly the same slope, whereas the slopes in electro-, muo- and photoproduction are definitely lower in the available range of relatively low W .

Fig. 4 gives again $\langle n \rangle$, the dispersion D ($D^2 = \langle n^2 \rangle - \langle n \rangle^2$) and the ratio $\langle n \rangle / D$ vs W^2 from ref. 9 together with the results from experiments on $p\bar{p}$ annihilation and on pp and π^+p scattering. For $\langle n \rangle$ and D the νp data points fall between the annihilation and hadron-hadron values. The $\langle n \rangle / D$ ratio drops for pp and π^+p scattering whereas it is roughly constant (~ 2.6) for νp in the entire W range. Fig. 5 shows $\langle n \rangle \cdot P(n, W)$ vs $n / \langle n \rangle$ for various intervals of W . It is seen that Koba-Nielson-Olesen (KNO) scaling 13 is well fulfilled (i. e. the points for the various W fall on the same curve) and that there is remarkable similarity with KNO scaling in $p\bar{p}$ annihilation whereas the KNO curve for high-energy pp scattering is much wider. A simple explanation of this result may be based on the fact that in hadron-hadron interactions diffraction scattering contributes ($\sim 20\%$) with low-multiplicity events at all energies (thus widening the multiplicity distribution), whereas diffraction scattering is absent in $p\bar{p}$ annihilation and very small in νp CC reactions 14.

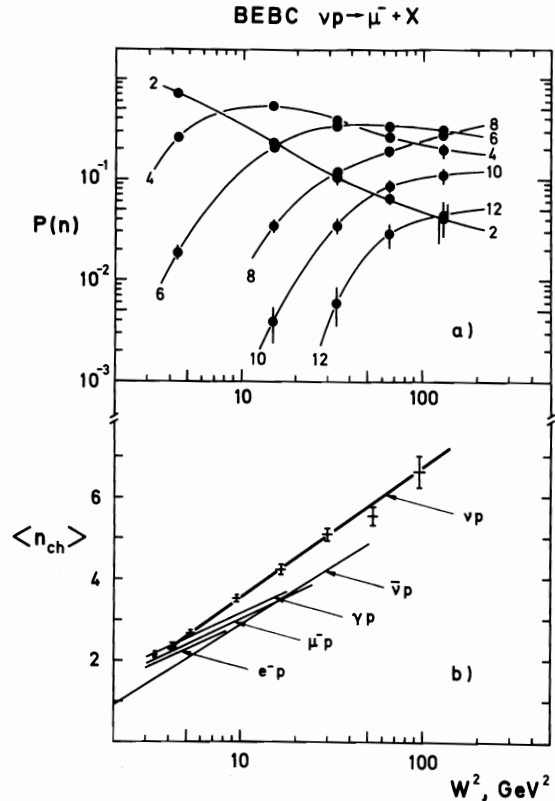


Fig. 3: (a) charged multiplicity probability $P(n, W)$ and (b) average charged multiplicity $\langle n \rangle$ of hadrons vs W^2 from BEBC νH_2 9. The curves in (a) are drawn to guide the eye. The straight lines in (b) are fits of the form $\langle n \rangle = a + b \cdot \ln W^2$ to the νp data points and to results from other leptonproduction experiments: $\bar{\nu}_p$ 4, e^-p 10, μ^-p 11, γp 10,12. The fitted values for a and b are compiled in Table 2.

Table 2: Values for a and b obtained from fitting $\langle n \rangle = a + b \cdot \ln W^2$ (W in GeV) to the average charged multiplicity $\langle n \rangle$ measured in various leptonproduction experiments.

Reaction	Hadronic Charge	W^2 range (GeV ²)	a	b	Ref.
νp	2	4-140 4-100	0.38 ± 0.07	1.38 ± 0.03 1.35 ± 0.15	9 6
$\bar{\nu}_p$	0	1-50	0.06 ± 0.06	1.22 ± 0.03	4
e^-p	1	3-8, $\langle q^2 \rangle = 0.78$ GeV ²	0.85 ± 0.09	0.88 ± 0.05	10
μ^-p	1	3-25, $q^2 \geq 0.24$ GeV ²	0.89 ± 0.14	0.92 ± 0.07	11
γp	1	3-18	1.10 ± 0.13	0.89 ± 0.06	10,12

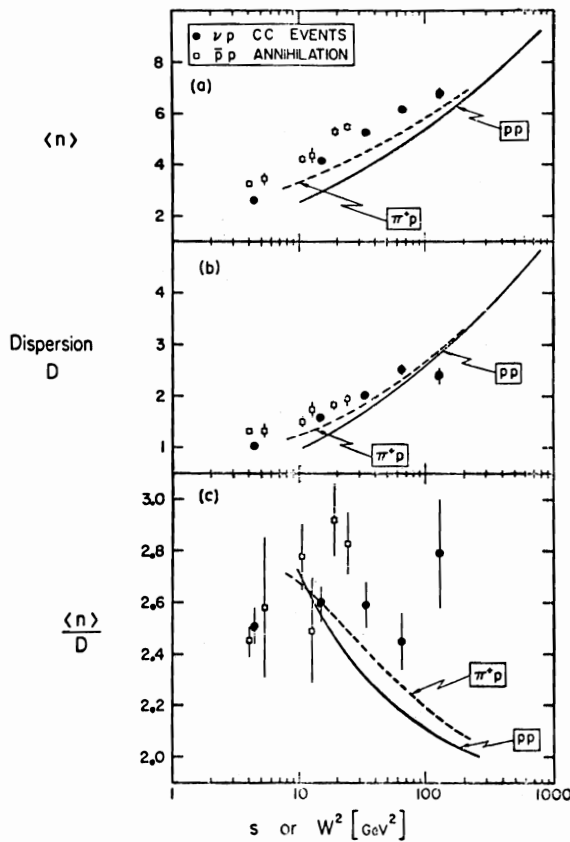


Fig. 4: (a) average charged multiplicity $\langle n \rangle$, (b) dispersion D and (c) $\langle n \rangle / D$ vs W^2 or s from BEBC νH_2 ⁹. Shown are also results from $p\bar{p}$ annihilation (\square) and from π^+p and pp scattering (curves).

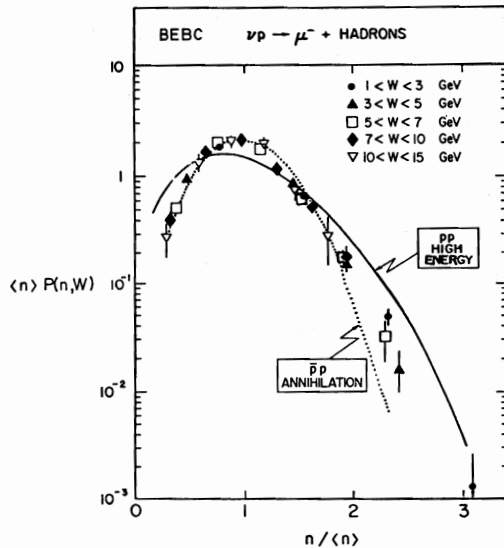


Fig. 5: KNO-scaling distribution of $\langle n \rangle P(n, W)$ vs $n / \langle n \rangle$ for 5 intervals of W from BEBC νH_2 ⁹. Shown are also KNO curves to the data of high energy pp scattering and $p\bar{p}$ annihilation.

B.) Longitudinal properties of single hadrons

1.) x_F distributions

Feynman scaling has been observed⁵ for $\bar{\nu}N$ scattering (i.e. in $W^-N \rightarrow h^+ + X$). This is confirmed now for νp scattering (i.e. in $W^+p \rightarrow h^+ + X$)⁹: Fig. 6 shows the normalized Lorentz-invariant cross section (integrated over p_T) $\frac{1}{N_{ev}} \frac{2}{\pi} \frac{E}{W} \frac{dN^{\pm}}{dx_F}$ vs x_F for positive and negative hadrons for low and high W and q^2 . The distributions are seen to be independent of W or q^2 , although for negative hadrons the cross section seems to be somewhat larger for high than for low W or q^2 around $x_F = 0$.

2.) Rapidity distributions

After having discussed some general features of the hadronic final state we now turn to more specific comparisons of the data with the naive QPM. For the experimentalist these questions arise:

- How well can one separate the target from the current fragments? This question is investigated with data from the 15' $\bar{\nu}H_2$ experiment in some detail in ref. 15.
- In which system (cms or Breit system) should one carry out such a separation by taking those particles as current fragments which go forward (i.e. in current direction) in the respective system ($x_F > 0$ or $z_B > 0$)?

For a large rapidity range $\Delta y \approx \ln W^2$ (W in GeV) the various regions are well separated from each other as shown schematically in Fig. 7 (taken from ref. 16, see also e.g. ref. 17). Allowing a Δy interval of at least 1.5 units for each fragmentation region, a reasonable separation becomes possible only for W above 4.5 GeV, whereas most events in present neutrino experiments are at lower W , as can be seen from the W distributions of the BEBC νH_2 ⁹ and the 15' $\bar{\nu}H_2$ ¹⁵ experiments in Fig. 8. Many physics investigations carried out at present with experimental data on neutrino-production are handicapped by this limitation in W and q^2 .

Fig. 9 shows the cms rapidity y^* distribution from the 15' $\bar{\nu}H_2$ experiment¹⁵ of positive and negative hadrons and of their difference (charge distribution) for $W > 4$ GeV and $q^2 > 1$ GeV². The y distributions from the BEBC νH_2 experiment⁹ in the cms and in the lab are given for 3 intervals of W in Fig. 10. Both figures show that at high W a plateau seems to develop. Thus an attempt to separate target and current fragments may become successful above $W \approx 4$ GeV whereas for lower W there is strong overlap. This is supported by Fig. 11 from the 15' $\bar{\nu}H_2$ experiment¹⁵ which shows the charge ratio $\frac{N^+}{N^-}$ vs z for $W^2 \gtrsim 10$ GeV². For large W the ratio drops for $z \rightarrow 1$ in qualitative agreement with the QPM (the leading meson from d-quark fragmentation

BECB $\nu p - \mu^- h^\pm X$

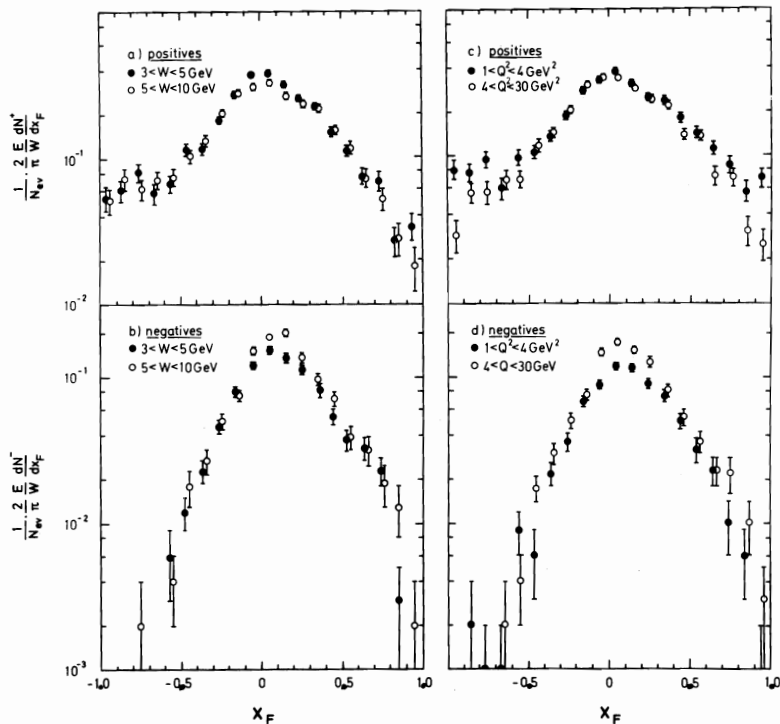


Fig. 6: Normalized Lorentz-invariant semi-inclusive cross-section for positive (a,c) and negative (b,d) hadrons h^\pm in $\nu p \rightarrow \mu^- h^\pm X$ from BECB νH_2^9 vs x_F , for 2 intervals of W (a,b) and of q^2 (c,d).

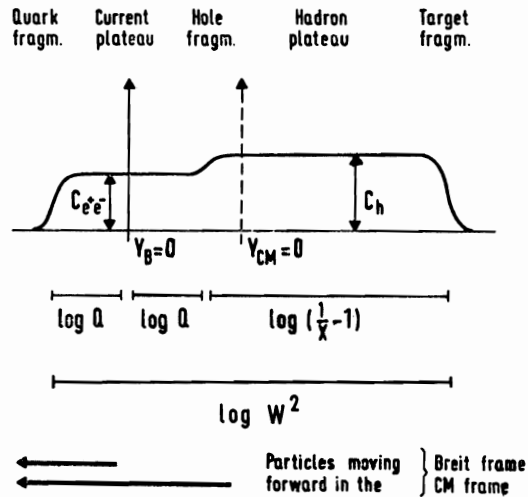


Fig. 7: Schematic rapidity distribution defining the various rapidity regions in deep inelastic lepto-production (from ref. 16).

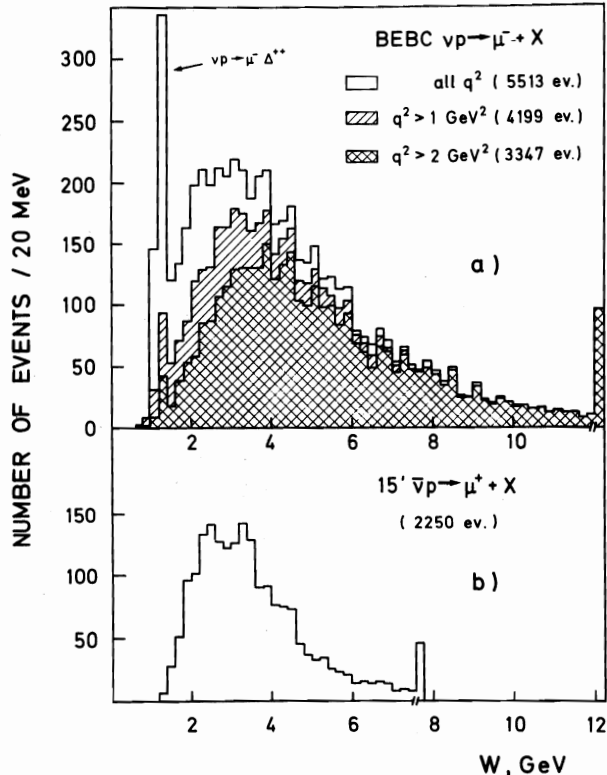


Fig. 8: Distribution of the hadronic effective mass W (a) from BECB νH_2^9 and (b) $15' \bar{\nu} H_2^{15}$. The single hatched (double hatched) distributions in (a) are for $q^2 > 1 \text{ GeV}^2$ (2 GeV^2).

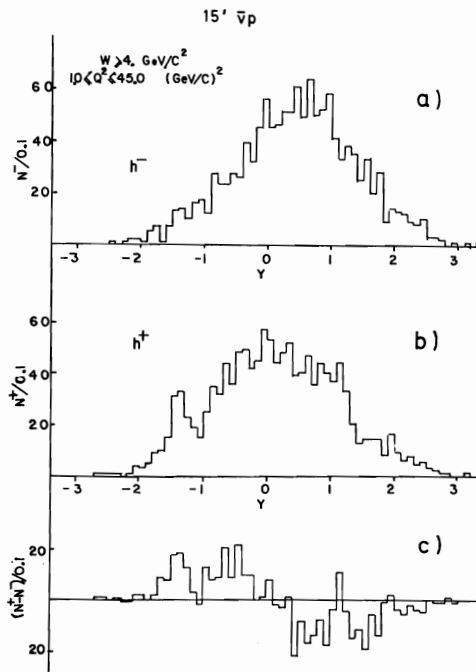


Fig. 9: Single-particle rapidity distribution in the hadronic cms for (a) negative hadrons, (b) positive hadrons, and (c) the difference (charge) for $W > 4 \text{ GeV}$ and $q^2 > 1 \text{ GeV}^2$ from $15' \bar{\nu} H_2^{15}$.

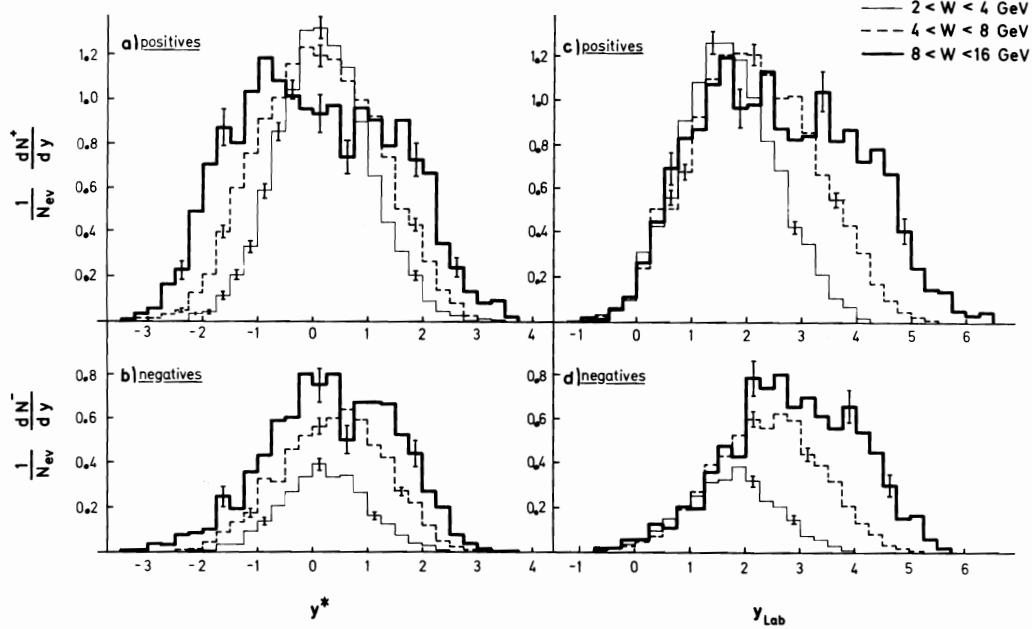


Fig. 10: Rapidity distributions (particles per event and unit rapidity) in the cm system (a,b) and in the lab system (c,d) for positive (a,c) and negative (b,d) hadrons for three W intervals from BEBC νH_2 ⁹. Typical statistical uncertainties are indicated by the error bars.

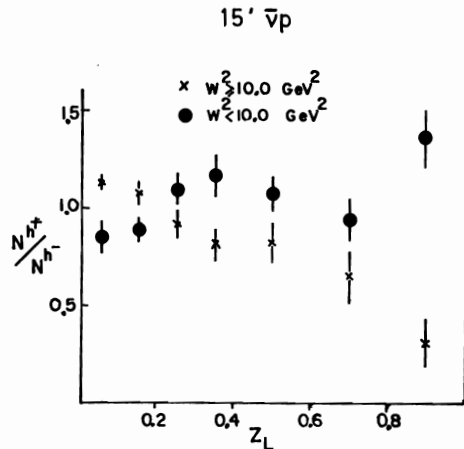


Fig. 11: Ratio of positive to negative hadrons vs $z_L = E_h/v$ for $W^2 < 10 \text{ GeV}^2$ (\bullet) and $W^2 > 10 \text{ GeV}^2$ (\times) from $15' \nu H_2$ ¹⁵.

is most often a π^- , (charge-retention effect⁸), whereas for small W no such tendency is observed.

As for the second question above one may hope to learn something by looking at the charge distribution in rapidity. Fig. 9c shows a definite step in this distribution around $y^* = 0$. An equally pronounced step around $y^* = 0$ is observed for high W in the BEBC νH_2 data⁹ in Fig. 12, which shows the charge dis-

tributions in cms, lab and Breit-system rapidity for 3 intervals of W. In the lab and Breit system the step occurs around $y_{\text{Lab}} = 2$ and $y_{\text{Breit}} = -1$ respectively. This result seems to indicate that the separation between current and target fragments is most appropriately carried out in the hadronic cm system and not in the Breit frame.

3.) Charge distributions and total net charges $\langle Q_q \rangle$

If one sums the charges of all hadrons from the fragmentation of a quark q one obtains the integer total net charge Q_q of the quark jet. Neglecting fragmentation into baryons, Field and Feynman⁸ and others before¹⁸ have shown that the average of Q_q over many q-jets (which is the integral over the difference of the fragmentation functions of quark q into positive and negative mesons) is related to the charge e_q of quark q by

$$\begin{aligned} \langle Q_q \rangle &\equiv \int_0^1 [D_q^+(z) - D_q^-(z)] dz \\ &= e_q - \sum_a \gamma_a e_a = e_q - e_{\langle q \rangle} \end{aligned} \quad (9)$$

Here γ_a is the probability for creating a quark-antiquark pair $a\bar{a}$ from the "sea"; the constant correction term ("charge leakage") $e_{\langle q \rangle} \equiv \sum_a \gamma_a e_a$ is the charge of an "average" quark $\langle q \rangle$ created from the sea. Relation (9)

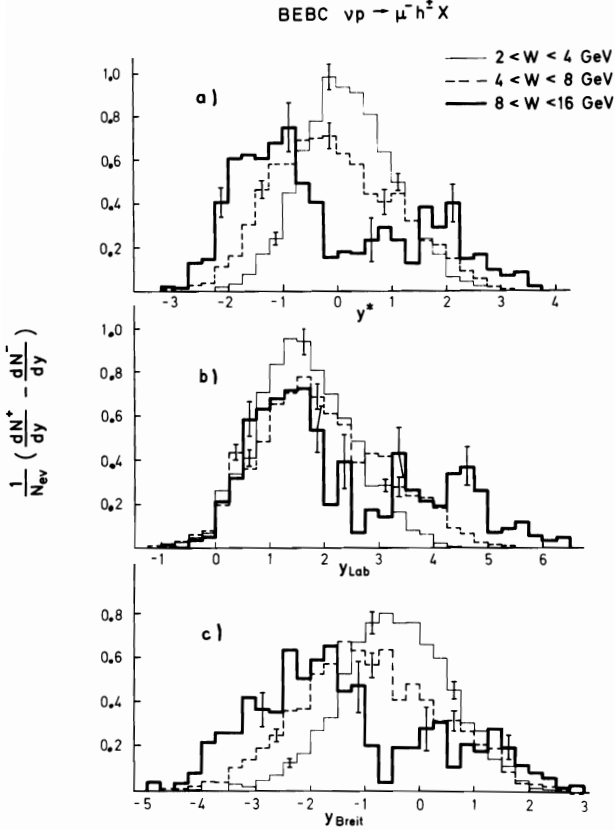


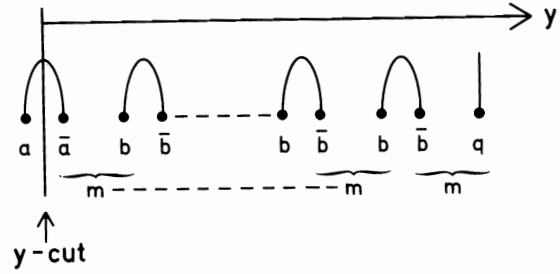
Fig. 12: Rapidity distribution of charge per event and unit rapidity vs rapidity in the hadronic cms (a), the lab system (b) and the Breit system (c) for 3 intervals of W from BEBC vH_2 ⁹. Typical statistical uncertainties are indicated by the error bars.

becomes directly obvious from the rapidity diagram in Fig. 13: Since in measuring Q_q one collects mesons m , the last pair $a\bar{a}$ in the chain has to be split and the charge of a , occurring with weight γ_a , must be subtracted. The neutral $b\bar{b}$ pairs between q and \bar{a} do not contribute to Q_q .

It should be pointed out that because of the a priori unknown constant $e_{\langle q \rangle}$ in (9) a measurement of $\langle Q_q \rangle$ gives the quark charges only up to this constant, i.e. without further assumptions only differences

$$\langle Q_q \rangle - \langle Q_{q'} \rangle = e_q - e_{q'} \quad (10)$$

of quark charges can be measured, not the quark charges themselves¹⁹. This is true even if the γ_a were known, since the quark charges occur in $e_{\langle q \rangle}$. In fact, neglecting the production of heavy mesons containing c quarks ($\gamma_c = 0$) and using $\gamma_u + \gamma_d + \gamma_s = 1$, it follows from the minimum assumptions $e_u - e_d = 1$ (π^+) and $e_u - e_s = 1$ (K^+) that



$$\langle Q_q \rangle = e_q + \sum_a \gamma_a e_{\bar{a}} = e_q - \sum_a \gamma_a e_a$$

Fig. 13: Schematic rapidity diagram showing how the average net hadron charge $\langle Q_q \rangle$ is composed of quark charges.

$$\langle Q_u \rangle = 1 - \gamma_u, \quad \langle Q_d \rangle = \langle Q_s \rangle = -\gamma_u, \quad (11)$$

$$e_{\langle q \rangle} = e_u - 1 + \gamma_u$$

Thus the total net charges $\langle Q_q \rangle$ are independent of the quark charges; they measure the probability $\gamma_u!$ For SU(2) symmetry

$$\gamma_u = \gamma_d = \gamma, \quad \gamma_s = 1 - 2\gamma \quad (12)$$

and for an SU(3)-symmetric sea

$$\gamma_u = \gamma_d = \gamma_s = \gamma = \frac{1}{3}. \quad (13)$$

With the normal charge assignments to the quarks one obtains

$$e_{\langle q \rangle} = \gamma_u - \frac{1}{3} (= 0 \text{ for an SU(3)-symmetric sea}) \quad (14)$$

A clean measurement of $\langle Q_u \rangle$ in v reactions and of $\langle Q_d \rangle$ in \bar{v} reactions at finite W is difficult for two reasons:

- At small Bjorken x sea quarks in the nucleon contribute to the reaction so that one is not collecting the fragments of just one flavor. Therefore one should exclude events with too small x values.
- As discussed above it is not clear if one should make the selection of current fragments in the cms ($x_F > 0$) or in the Breit frame ($z_B > 0$) and in any case there is overlap at finite W , i.e. loss of current fragments into the backward hemisphere and contamination from target fragments in the forward hemisphere. In order that the target fragments be well separated from the current fragments in rapidity, $\ln q^2$ and $\ln W^2 - \ln q^2$ should be large, see Fig. 7.

Both requirements of larger x and large W^2/q^2 are in conflict with each other because of equ. (3b).

A careful determination of $\langle Q_d \rangle$ has been carried out by the 15' $\bar{v}Ne-H_2$ collaboration²⁰ by extrapolating to $W = \infty$ in order to remove

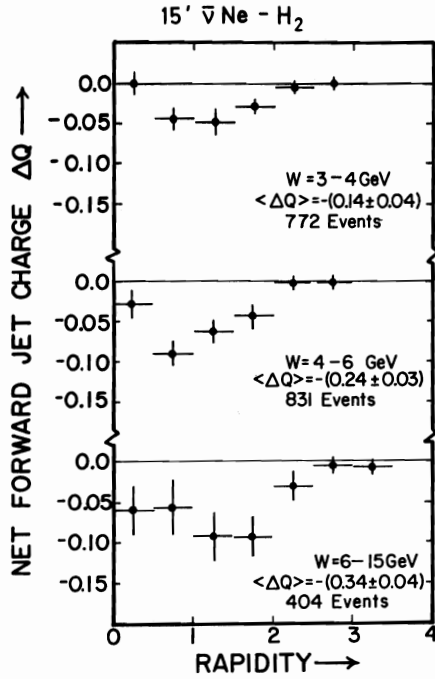


Fig. 14: Distribution of charge per event in cms rapidity for hadrons going forward in the cms ($y > 0$) in events with $x > 0.1$ and $q^2 > 1 \text{ GeV}^2$ for three intervals of W . Given also are the values of the total net charge $\langle Q \rangle$ of forward going hadrons. From $15' \bar{\nu} \text{ Ne-H}_2^{20}$.

the overlap mentioned above. Fig. 14 shows for $x > 0.1$ and $q^2 > 1 \text{ GeV}^2$ the net-charge distributions in cms rapidity for three intervals of W together with the values obtained for the total net charge $\langle Q \rangle$ going forward in the hadronic cms. The absolute values of $\langle Q \rangle$ increase with W ; they are plotted vs W^{-1} in Fig. 15 where an extrapolation linear in W^{-1} is carried out towards $W^{-1} = 0$ (this extrapolation in W^{-1} is justified by a correlation-length argument). The extrapolated value at $W = \infty$ is $\langle Q_d \rangle = -0.46 \pm 0.08$ which gives $\gamma_u = 0.46 \pm 0.08$ according to (11). A similar (preliminary) analysis with data from the BEBC νH_2 experiment⁹ is shown in Fig. 16: For $q^2 > 1 \text{ GeV}^2$ and $x > 0.1$ the net charge is plotted vs W^{-1} for hadrons going forward in the cms or in the Breit frame. The extrapolated values obtained from linear fits to the first six points are $\langle Q_u \rangle = 0.59 \pm 0.10$ (i.e. $\gamma_u = 0.41 \pm 0.10$) for $x_F > 0$ and $\langle Q_u \rangle = 0.52 \pm 0.08$ (i.e. $\gamma_u = 0.48 \pm 0.08$) for $z_B > 0$.

Two other determinations of $\langle Q_u \rangle$ and $\langle Q_d \rangle$ have been carried out recently by using ν and $\bar{\nu}$ reactions in BEBC (Ne-H₂, ref. 21) and the 15' chamber (H₂, ref. 15). In both experiments the charge of all hadrons going forward in the Breit frame is collected and no extrapolation to infinite W is carried out. The results from all four experiments are compiled

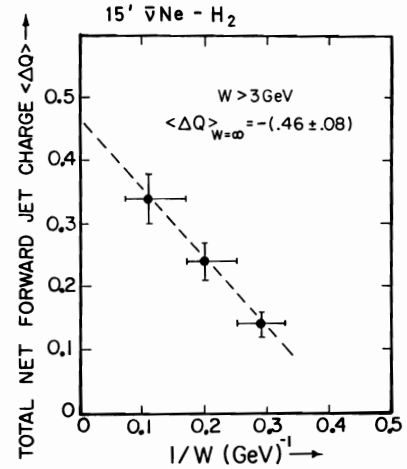


Fig. 15: Total net charge $\langle Q \rangle$ per event of hadrons going forward in the cms vs $1/W$ from $15' \bar{\nu} \text{ Ne-H}_2^{20}$. The dashed line shows a linear fit to the three points extrapolating to a value of $\langle Q \rangle_{W=\infty} = -0.46 \pm 0.08$.

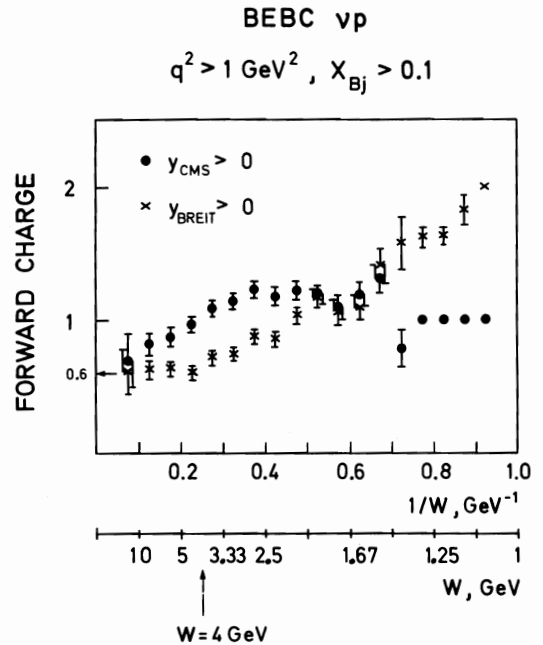


Fig. 16: Total net charge $\langle Q \rangle$ of hadrons going forward in the cms (\bullet) or Breit system (\times) vs $1/W$ from BEBC νH_2 ⁹ (preliminary).

in Table 3. The values obtained for γ_u agree well amongst each other, thus supporting the QPM, apart from those derived from $\langle Q_d \rangle$ in the last two experiments. Here the rather low absolute values measured for $\langle Q_d \rangle$ most likely come from the finite W values and from selecting in the Breit system. In fact it is seen in Fig. 17 from the $15' \bar{\nu} \text{H}_2$ experiment¹⁵ that the absolute value of $\langle Q_d \rangle$ increases (as in Fig. 15) with W and that it is larger for the cms selection ($x_F > 0$) than for the Breit-frame

Table 3 Measured total net charges $\langle Q_u \rangle$, $\langle Q_d \rangle$ and derived probability γ_u using $\gamma_u = 1 - \langle Q_u \rangle = -\langle Q_d \rangle$, see equ. (11).

Selection	neutrino		antineutrino		experiment, ref.
	$\langle Q_u \rangle$	γ_u	$\langle Q_d \rangle$	γ_u	
$W = \infty, x > 0.1, q^2 > 1 \text{ GeV}^2, x_F > 0$			-0.46 ± 0.08	0.46 ± 0.08	$15' \bar{\nu} \text{Ne-H}_2$ ²⁰
$W = \infty, x > 0.1, q^2 > 1 \text{ GeV}^2$	$x_F > 0$	0.59 ± 0.10	0.41 ± 0.10		BEBC νH_2 ⁹
	$z_B > 0$	0.52 ± 0.08	0.48 ± 0.08		
$W > 4 \text{ GeV}, x > 0.1, z_B > 0$	0.55 ± 0.06	0.45 ± 0.06	-0.12 ± 0.13	0.12 ± 0.13	BEBC $\nu, \bar{\nu} \text{Ne-H}_2$ ²¹
$W > 4 \text{ GeV}, q^2 > 1 \text{ GeV}^2, z_B > 0$	0.55 ± 0.07	0.45 ± 0.07	-0.18 ± 0.05	0.18 ± 0.05	$15' \nu, \bar{\nu} \text{H}_2$ ¹⁵

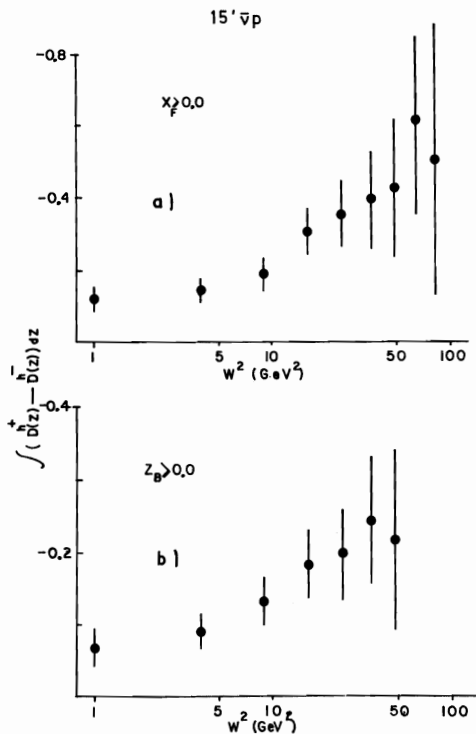


Fig. 17: Total net charge of hadrons going forward (a) in the cms and (b) in the Breit system for events above W^2 from $15' \bar{\nu} \text{H}_2$ ¹⁵.

selection ($z_B > 0$) although the errors are rather large at high W .

The probability $\gamma = \gamma_u$ can also be determined from the ratio γ_s/γ_d which is directly obtained e.g. as the K^\pm/π^\pm ratio at high fractional energy z (e.g. $D^K(z)/D^\pi(z) \xrightarrow{z \rightarrow 1} \gamma_s/\gamma_d$) as measured in high-energy collisions, or as the branching ratio $\psi \rightarrow KK^*/\psi \rightarrow \pi\rho$ after phase space correction. Values around $\gamma_s/\gamma_d \approx 0.5$ are obtained ^{8,20} yielding $\gamma \approx 0.4$ according to (12).

4.) Fragmentation functions and their moments

a.) New measurements. Fragmentation functions $D_q^\pm(z)$ of quarks q into positive or negative hadrons h^\pm , where z is the energy fraction of q carried by h^\pm , have been measured by the various groups ^{9,15,20,22-24}. Neglecting sea quarks, $q = u(d)$ in $\nu(\bar{\nu})$ reactions. The histograms in Fig. 18 show the D-functions for (a) $\nu \rightarrow h^+$ and (b) $\nu \rightarrow h^-$ on protons and neutrons from the $15' \nu \text{D}_2$ experiment ²³ for $W > 4 \text{ GeV}$ and $q^2 > 2 \text{ GeV}^2$. Added on to the figure are the results for $\nu \rightarrow h^+$, $\bar{\nu} \rightarrow h^-$ in (a) and for $\nu \rightarrow h^-, \bar{\nu} \rightarrow h^+$ in (b) from the other experiments with similar cuts on W and q^2 . It is seen that the proton and neutron data agree with each other within statistics, as predicted by the QPM. Furthermore there is rough agreement amongst the various experiments. For pions the D-functions for $\nu \rightarrow h^\pm$ and $\bar{\nu} \rightarrow h^\mp$ should be equal due to isospin symmetry. An observed excess of h^+ over h^- is probably due to protons in the h^+ sample.

b.) Universality. The naive QPM predicts D_q^h to be independent of the process in which the fragmenting quark q is created (factorisation, universality, environmental independence ²⁵⁻²⁷). Therefore the same D-functions D_q^h occur in the various leptonproduction processes and in e^+e^- annihilation, although with different weights ²⁷. However, assuming charge-conjugation invariance and isospin symmetry one obtains for the z distributions of positive and negative pions per event in the various processes the following simple relation ²⁶:

+) The p_T dependence of fragmentation functions is not considered in this section.

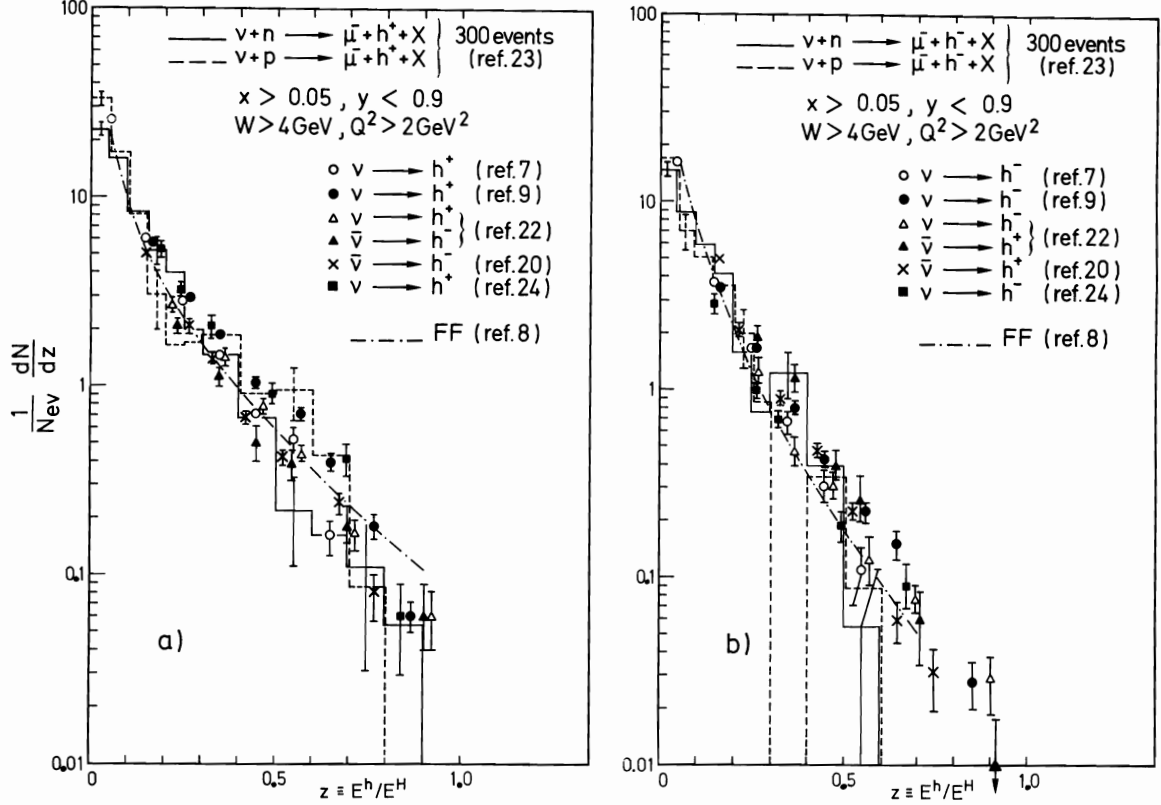


Fig. 18: Compilation of fragmentation functions for (a) $\nu + h^+$, $\bar{\nu} + h^-$ and (b) $\nu + h^-$, $\bar{\nu} + h^+$ from various experiments.

$$\begin{aligned}
 [N^{\pi^+}(z) + N^{\pi^-}(z)]_{\nu N} &= [N^{\pi^+}(z) + N^{\pi^-}(z)]_{\bar{\nu} N} = \\
 [N^{\pi^+}(z) + N^{\pi^-}(z)]_{eN, \mu N} &= \frac{5}{6} [N^{\pi^+}(z) + N^{\pi^-}(z)]_{e^+e^-} \quad (15) \\
 &= D_u^{\pi^+}(z) + D_u^{\pi^-}(z)
 \end{aligned}$$

Here the fragmentation of s-quarks into pions has been neglected and in e^+e^- annihilation pions are taken per hemisphere. Since most charged particles are pions the z distributions of charged hadrons should roughly agree with each other in all processes. This prediction of the QPM is in good agreement with the experimental results as can be seen in Fig. 19, taken from ref. 7,20.

c.) Factorisation and scaling. We now discuss the question of factorisation and scaling of the z distributions. In general the semi-inclusive νp charged-current cross section can be written as

$$\begin{aligned}
 \frac{d\sigma^h}{dx dq^2 dz}(x, q^2, z) &= \frac{d\sigma_{ev}}{dx dq^2}(x, q^2) \cdot D^h(z, x, q^2) \quad (16) \\
 &= \frac{G^2}{2\pi} \frac{F(x, q^2)}{x} \cdot D^h(z, x, q^2)
 \end{aligned}$$

where $\frac{d\sigma_{ev}}{dx dq^2}$ is the event cross section and $F = F_2 = 2xF_1 = xF_3$ is assumed. If h is a current fragment then the naive QPM predicts factorisation in x and z for fixed q^2 , i.e.

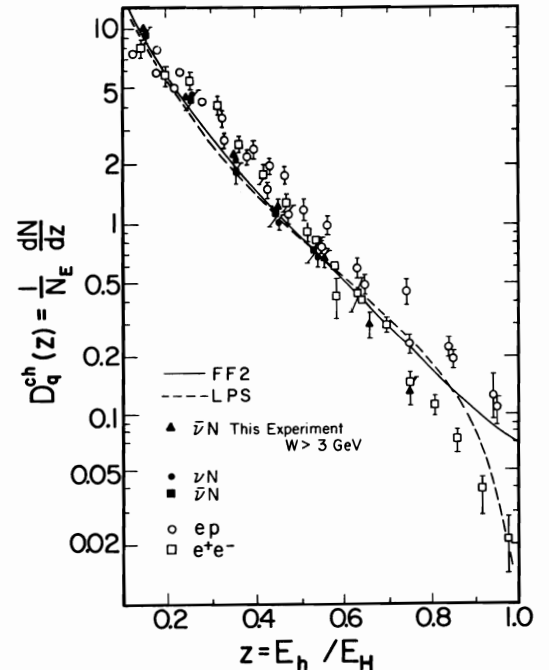


Fig. 19: z distributions of charged hadrons per event (in e^+e^- per hemisphere) in νN , $\bar{\nu} N$ and ep scattering and in e^+e^- annihilation together with the predictions of Field and Feynman⁶ and of a longitudinal phase space (LPS) model⁷. Figure from ref. 7,20.

$D^h(z, x, q^2) = D^h(z, q^2)$, and scaling, i.e. $D^h(z, q^2) = D^h(z)$. These predictions are modified by quantum chromodynamics (QCD). In QCD, the D-functions become q^2 dependent (scaling violation) due to gluon emission according to the diagrams in Fig. 20. The q^2 dependence of the D-functions has been calculated to 1st order in perturbative QCD by Owens and Uematsu²⁸ using the Altarelli-Parisi method²⁹ (see below). As for factorisation, it is predicted by perturbative QCD in leading order whereas in the next-to-leading order violation of factorisation is expected as recently calculated by Sakai³⁰, Altarelli et al.³¹ and Baier and Fey³².

Factorisation and scaling have been investigated experimentally by the BEBC νH_2 collaboration^{9,33} with relatively high statistics (~ 5600 CC events). The D-functions (z -distributions) of positive and negative hadrons are given by

$$D^\pm(z, q^2) = \frac{1}{N_{ev}(q^2)} \cdot \frac{dN^\pm}{dz}(z, q^2) \quad (17)$$

and their moments by

$$D^\pm(m, q^2) = \int_0^1 z^{m-1} D^\pm(z, q^2) dz. \quad (18)$$

Here $N_{ev}(q^2)$ is the number of events at q^2

+) Factorisation follows from the fact that in νp charged current reactions only a single quark flavor is involved ($d \rightarrow u$) if one neglects the contributions from sea quarks. The Cabibbo suppressed sea quark contributions $s \rightarrow u$ and $\bar{u} \rightarrow \bar{s}$ can indeed be neglected. The contribution from $\bar{u} \rightarrow \bar{d}$ should not disturb factorisation since most of the secondary hadrons are pions for which $D_{\bar{d}}^{\pi^\pm} = D_u^{\pi^\pm}$ holds.

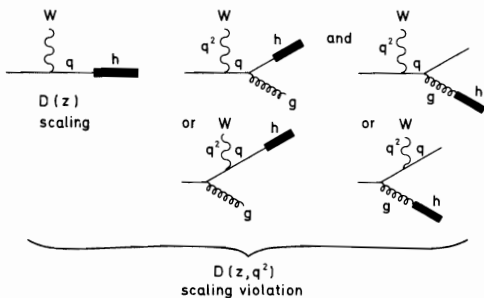


Fig. 20: QCD diagrams (gluon emission) causing scaling violation of fragmentation functions.

and N^\pm the number of positive or negative tracks in these events. z is taken as $z = E_h/E_H$ in the lab system (see (4)). Fig. 21 shows for all W the distributions $D^\pm(z, q^2)$ vs z for low and high q^2 for all x_F and for $x_F > 0$. The cut $x_F > 0$ in the cms is made to select (at least approximately) the current fragments of the u quark so that D^\pm can be interpreted as the fragmentation functions D_u^\pm of the u quark. For $z \gtrsim 0.2$ there is practically no difference between the distributions with and without the x_F cut. This cut is applied in the subsequent Figs. 22-26. A significant q^2 dependence (scaling violation) is observed in Fig. 21; the distributions become narrower at high q^2 .

In order to investigate factorisation Fig. 22 shows as an example the 3rd positive moment vs x for three different intervals of q^2 . One observes factorisation (i.e. independence of x) at high q^2 , whereas at smaller q^2 the moment increases significantly with x implying non-factorisation in this q^2 region. Fig. 23 shows the 3rd positive moment (a) vs x and (b) vs q^2 for three intervals of W . For fixed W the values are rather independent of q^2 and (via equ. (3b)) of x which seems to indicate that the semi-inclusive cross section factorizes in x and z at fixed W and not at fixed (low) q^2 .

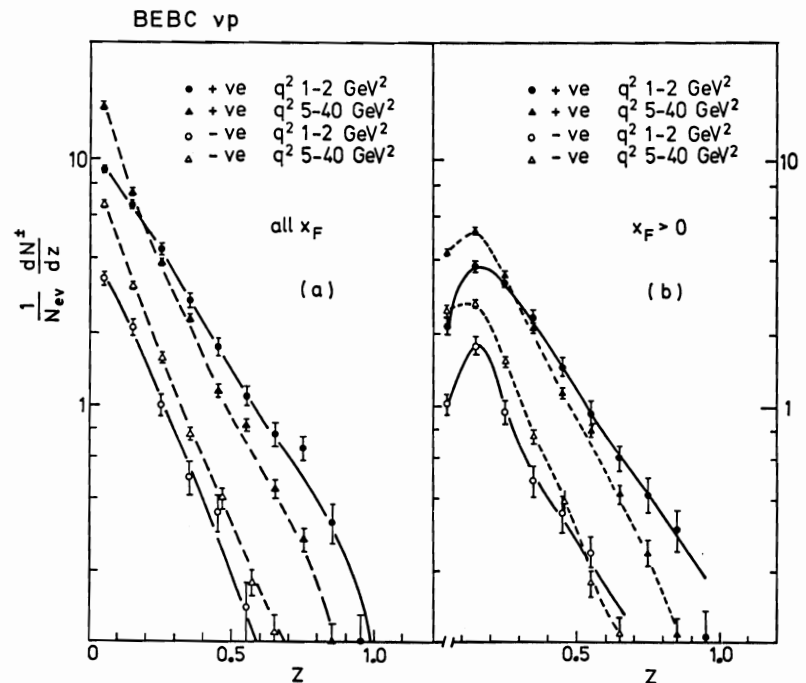


Fig. 21: z distributions ($z = E_h/E_H$) of positive and negative hadrons for two ranges of low and high q^2 from BEBC νH_2 ³³, (a) for all hadrons, (b) for hadrons going forward in the cms ($x_F > 0$). All W values are included. The curves are to guide the eye.

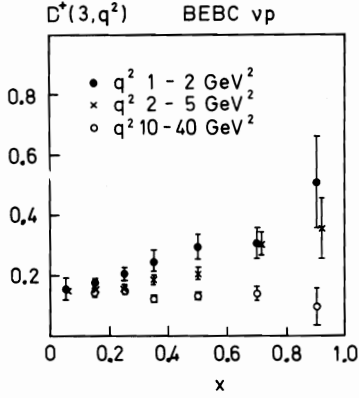


Fig. 22: Third fragmentation moment of positive hadrons with $x_F > 0$ vs Bjorken x for three intervals of q^2 , from BEBC νH_2 ³³.

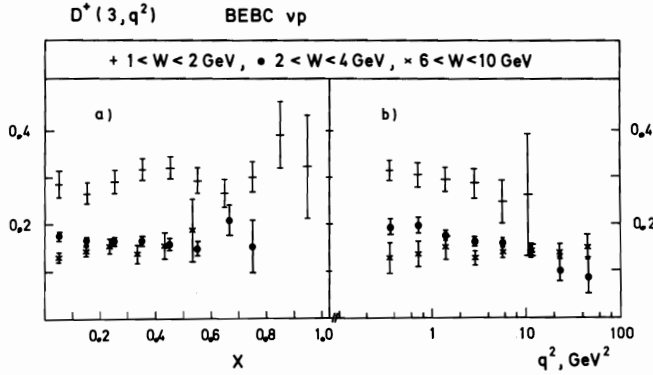


Fig. 23: Third fragmentation moment of positive hadrons with $x_F > 0$ (a) vs Bjorken x and (b) vs q^2 for three intervals of W , from BEBC νH_2 ³³.

d.) Non-singlet moments. The observed q^2 dependence has been compared with the 1st order QCD prediction²⁸ which is particularly simple for the non-singlet (NS) moments $D^{NS}(m, q^2)$, to which the gluon fragmentation (right-hand-side diagrams in Fig. 20) does not contribute:

$$D^{NS}(m, q^2) = C_m \left(\ln \frac{q^2}{\Lambda^2} \right)^{-d_m^{NS}} \quad (19)$$

where

$$d_m^{NS} = \frac{4}{33-2f} \left[1 - \frac{2}{m(m+1)} + 4 \sum_{j=2}^m \frac{1}{j} \right] \quad (20)$$

are the anomalous dimensions, f the number of flavors ($f = 3$ in this analysis), C_m unknown constants and Λ the scale parameter occurring in the running coupling constant $\alpha_s(q^2)$ of QCD. Experimentally

$$D_u^+ - D_u^- = D_{\bar{u}}^+ - D_{\bar{u}}^- = D^{NS} \quad (21)$$

is a non-singlet (where charge-conjugation invariance has been applied), irrespective of

the nature of the hadrons ($\pi^\pm, K^\pm, p/\bar{p}$). It follows from (19) that two NS-moments of order m_1 and m_2 are expected to fall on a straight line with slope $d_{m_2}^{NS}/d_{m_1}^{NS}$ when plotted against

each other on a log-log scale. Fig. 24 shows plots of $D^{NS} = D^+ - D^-$ and (for comparison) $D^+ + D^-$ for $m_1, m_2 = 4, 6$ and $3, 7$. In all cases the points fall on straight lines with fitted slopes as given in the figure. The slopes for the NS moments are in good agreement with the QCD prediction whereas the combinations $D^+ + D^-$ have substantially bigger slopes. In Fig. 25 the measured non-singlet moments for $m = 2, \dots, 7$ are shown vs q^2 for all W together with the result of a global fit (i.e. all m simultaneously) of equ. (19) to the data above $q^2 = 1 \text{ GeV}^2$ with C_m and Λ as free parameters. The QCD formula describes the data points very well and a value of $\Lambda = 0.54 \pm 0.08 \text{ GeV}$ is obtained. Fits have also been carried out for $q^2 > 2 \text{ GeV}^2$ and for all x_F . The Λ values obtained for the various selections are collected in Table 4; they give an impression of the uncertainty in the determination of Λ . Single fits for individual orders m show no statistically significant variation of Λ with m . Fig. 26 shows the same moments vs q^2 for $W > 4 \text{ GeV}$. No q^2 dependence is observed. Thus the q^2 dependence is observed only (Fig. 25) if low W values are included where the separation of current and target fragments is questionable. The good agreement with QCD is therefore perhaps surprising and may even be coincidental.

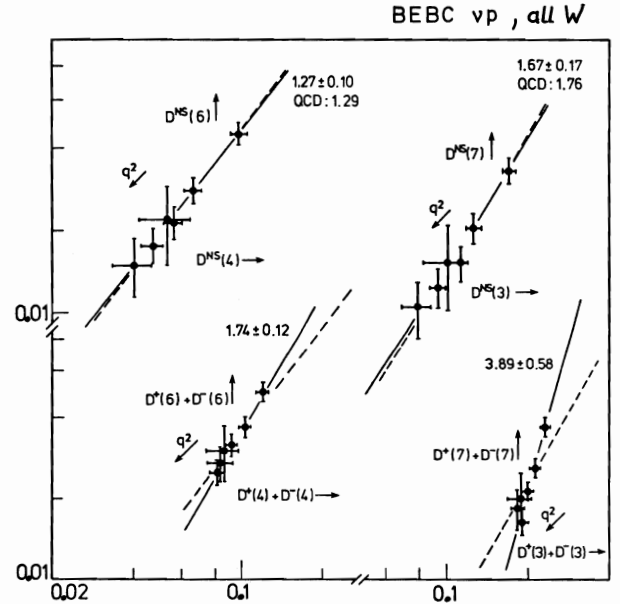


Fig. 24: Logarithmic plots of $m_2=6$ vs $m_1=4$ and $m_2=7$ vs $m_1=3$ non-singlet moments for $q^2 > 1 \text{ GeV}^2$, from BEBC νH_2 ³³. Shown are the combinations $D^+ - D^- = D^{NS}$ and $D^+ + D^-$. The full straight lines show the fitted slopes with values given in the figure, while the QCD-predicted slopes for non-singlet pairs are shown by the dashed lines. The errors indicated on each point are highly correlated. The independent errors are about half of those shown.

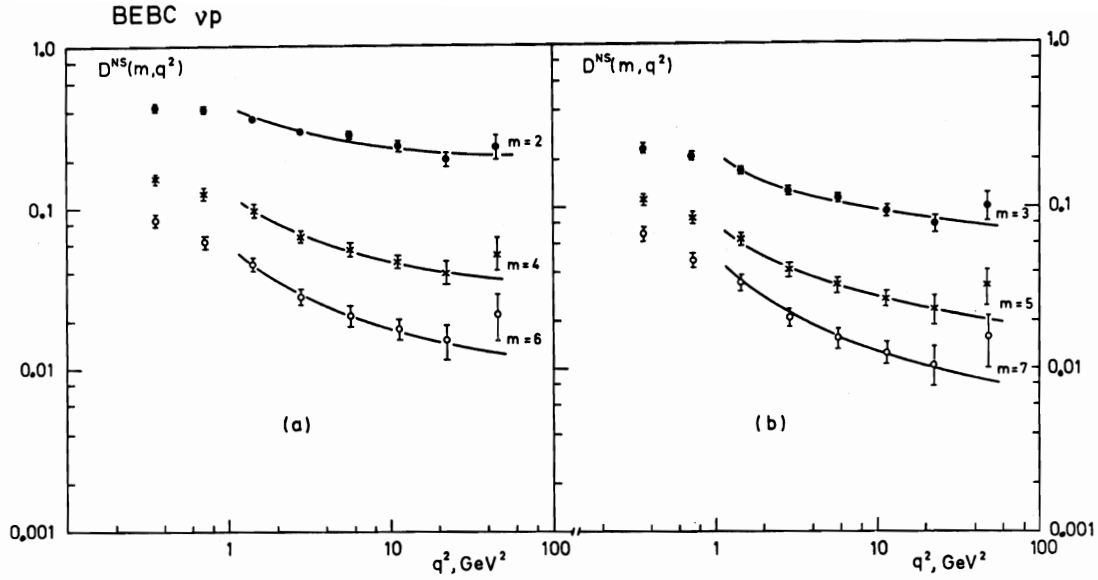


Fig. 25: Non-singlet moments for all W and $x_F > 0$ vs q^2 for $m=2, \dots, 7$ from BEBC νH_2 ³³. The curves show fits of the QCD formula (19) to the data points above $q^2 = 1 \text{ GeV}^2$.

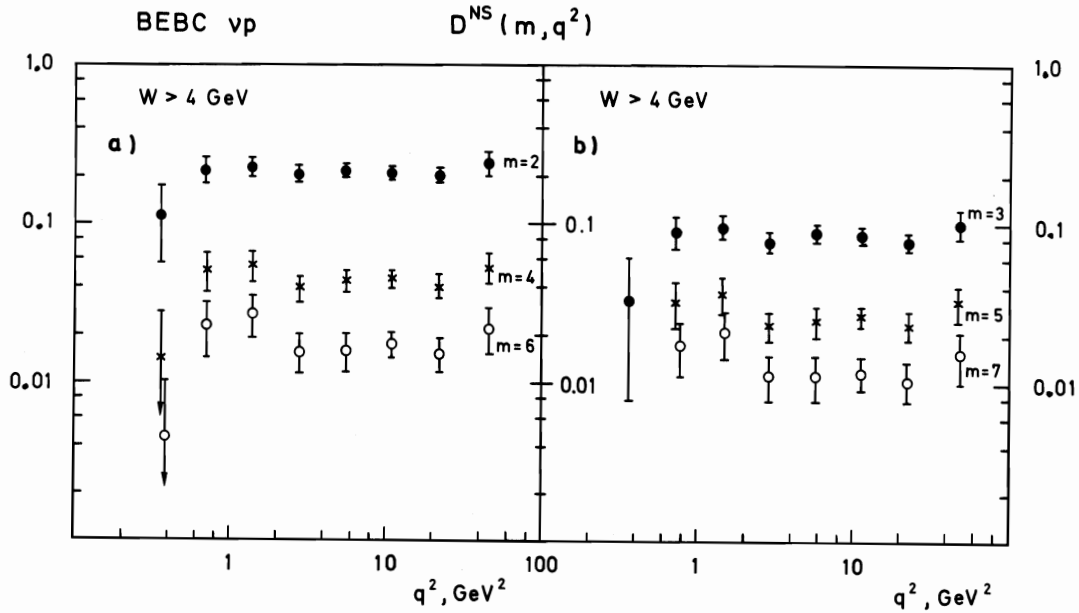


Fig. 26: Same as Fig. 25, but for $W > 4 \text{ GeV}$.

Table 4 Values of Λ (GeV) from global fits to $m = 2-7$ non-singlet moments

selection of secondaries	$q^2 > 1 \text{ GeV}^2$	$q^2 > 2 \text{ GeV}^2$
all	0.72 ± 0.07	0.62 ± 0.14
$x_F > 0$	0.54 ± 0.08	0.52 ± 0.15

The difficulty of separating the current and target fragments from each other at low W is emphasized by the $15' \bar{\nu}H_2$ collaboration¹⁵. Fig. 27 shows their z distribution for positive hadrons for low and high q^2 . For $W > 4$ GeV (a) scaling is observed, whereas for all W (b) the z distribution depends on q^2 . Although this is in qualitative agreement with the findings of the BEBC $\bar{\nu}H_2$ collaboration (Fig. 21), the authors attribute the apparent scaling violation in Fig. 27b to the overlap of current and target fragments at low W . It should be pointed out however that a cut in q^2 (as applied in the QCD analysis of ref. 33, see Table 4) removes a large fraction of low- W events (see hatched areas in Fig. 8a).

e.) Double moments. A more detailed study of non-factorisation is being carried out³⁴ with the data of the BEBC $\bar{\nu}H_2$ ⁹ collaboration by performing a double-moment analysis^{30,35}. The double moments of the fragmentation functions $D^h(z, x, q^2)$ in (16) are defined as

$$D^h(m, n, q^2) = \frac{\int_0^1 dx x^{n-1} \int_0^1 dz z^{m-1} \frac{d\sigma^h}{dx dq^2 dz}(x, q^2, z)}{\int_0^1 dx x^{n-1} \frac{d\sigma^{ev}}{dx dq^2}(x, q^2)} \quad (22)$$

$$= \frac{\int_0^1 dx x^{n-2} \int_0^1 dz z^{m-1} F(x, q^2) \cdot D^h(z, x, q^2)}{\int_0^1 dx x^{n-2} F(x, q^2)}$$

Factorisation implies that $D^h(m, n, q^2)$ does not depend on n . Two comments have to be made regarding the experimental evaluation of double moments:

- The event distribution in x and q^2 differs from the inclusive cross section due to the neutrino flux spectrum $\phi(E)$. This distortion is corrected for by using the obvious relations

$$\frac{d\sigma^{ev}}{dx dq^2}(x, q^2) = K \cdot \frac{dN^{ev}}{dx dq^2}(x, q^2) \Big/ \int_{q^2/2Mx}^{E_{max}} \phi(E) dE \quad (23)$$

$$\frac{d\sigma^h}{dx dq^2 dz}(x, q^2, z) = K \cdot \frac{dN^h}{dx dq^2 dz}(x, q^2, z) \Big/ \int_{q^2/2Mx}^{E_{max}} \phi(E) dE$$

so that the double moments become independent of the spectrum. Here E_{max} is the maximum neutrino energy of the spectrum, K a constant and $E_{min} = q^2/2Mx$ the minimum neutrino energy at which a given set of values (x, q^2) can be reached.

- For given q^2 the minimum x accessible is given by $x_{min} = q^2/2ME_{max}$ so that the x in-

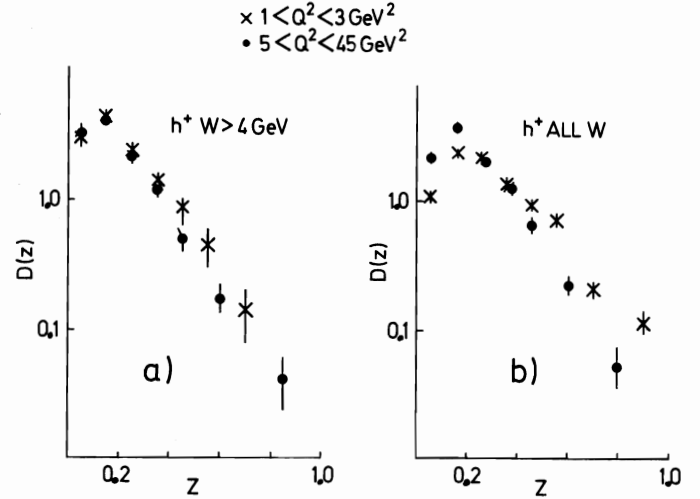


Fig. 27: z distributions ($z = E_h/\nu$) of positive hadrons with $x_F > 0$ for low and high q^2 from $15' \bar{\nu}H_2$ ¹⁵, (a) for $W > 4$ GeV and (b) for all W .

tegration in (22) can be carried out only from x_{min} and not from zero. The resulting bias should however be small for larger n and not too high q^2 .

In the actual analysis the well known Nachtmann variable ξ is used for x and the corresponding variable ζ (see equ. (5b)) is used for z . Only particles which go forward in the Breit frame are taken. The subsequent 3 figures show preliminary results³⁴. In Fig. 28 the non-singlet double moments are plotted vs q^2 for $m = 1, 2, 3, 5$ and $n = 1, 2, 3, 5$. The dashed lines are QCD predictions with $\Lambda = 0.75$ GeV, normalised to the $n=1$ data, and allow a comparison for different n . A significant n -dependence (i.e. non-factorisation) is observed at low q^2 , whereas at high q^2 the moments are less dependent on n . This is in agreement with the conclusion drawn already from Fig. 22. Fig. 29 shows log-log plots of $D^{NS}(m')$ vs $D^{NS}(m)$ for four different orders n together with the straight lines as predicted for NS-moments by QCD. The agreement with QCD is satisfactory, independent of n . This demonstrates that in spite of non-factorisation QCD is able to describe at least the predominant part of the observed q^2 dependence.

The approach to factorisation as $q^2 \rightarrow \infty$ has been calculated in next-to-leading order of QCD by Sakai³⁰. The following q^2 dependence of the ratio of two double moments with different values of n and the same m is predicted

$$R(m, n_1, n_2, q^2) \equiv \frac{D^{NS}(m, n_2, q^2)}{D^{NS}(m, n_1, q^2)} = 1 + \frac{A(m, n_1, n_2)}{\ln \frac{Q^2}{\Lambda^2}} \quad (24)$$

Formulae to compute the constants A are given in ref. 30. Fig. 30 shows four such

BEBC vp

DOUBLE MOMENTS : $D_U^{h^+}(M,N,q^2) - D_U^{h^-}(M,N,q^2)$ (non-singlet)

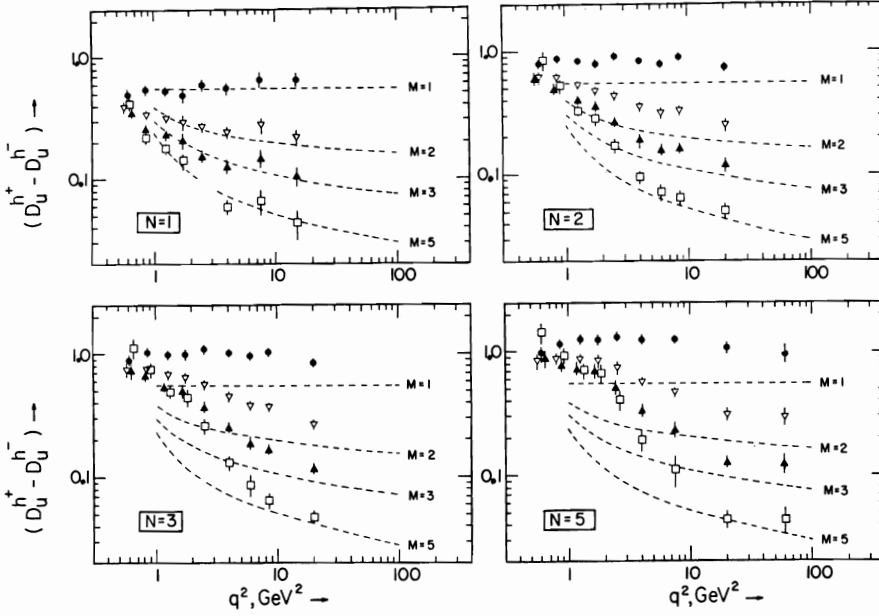


Fig. 28: Double non-singlet moments vs q^2 for $m = 1, 2, 3, 5$ and $n = 1, 2, 3, 5$ from BEBC νH_2 ^{9,34} for $z_B > 0$. The dashed curves are QCD predictions ($\Lambda = 0.75 \text{ GeV}$) normalised to the $n = 1$ data (preliminary).

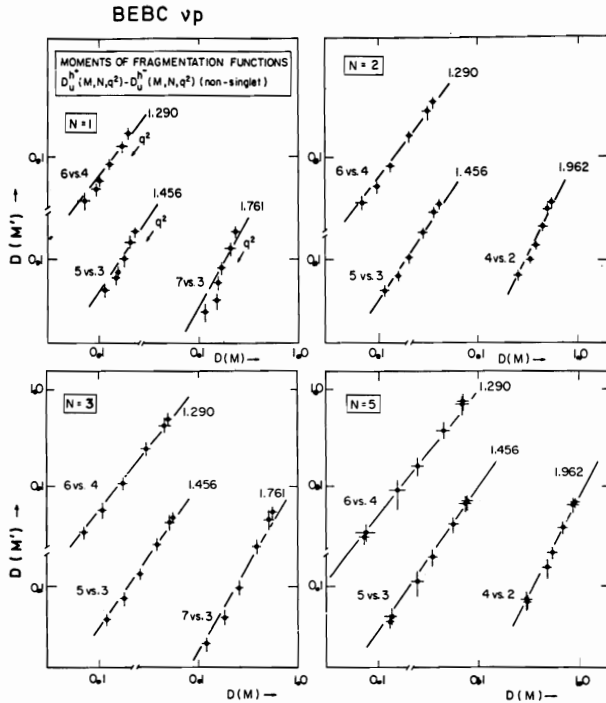


Fig. 29: Logarithmic plots of m' vs m double non-singlet moments for $n = 1, 2, 3, 5$ from BEBC νH_2 ^{9,34}. The straight lines and numbers give the slopes as predicted by QCD for non-singlet pairs (preliminary).

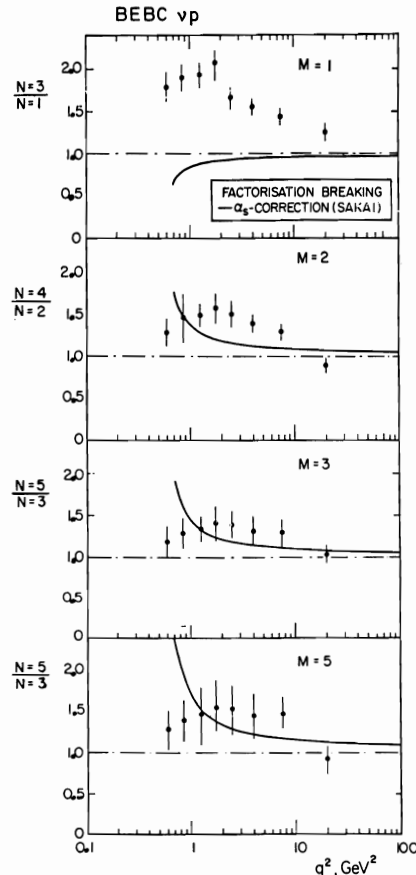


Fig. 30: Ratio of double non-singlet moments for different n and same m vs q^2 from BEBC νH_2 ^{9,34}. The curves show the non-factorisation predictions of QCD from ref. 30 (prelim.).

ratios vs q^2 together with the QCD-predicted curves. The data points show a tendency towards one for high q^2 , i.e. towards factorisation, although their quantitative agreement with theory is not so good. However, the experimental results on double moments are preliminary and further work is in progress.

f.) Quark-singlet moments and gluon moments

The following q^2 dependence is predicted by QCD²⁸ for the moments $D_{NS}^h(m, q^2)$ and $D_S^h(m, q^2)$ of a non-singlet and quark-singlet fragmentation function respectively:

$$\begin{aligned} D_{NS}^h(m, q^2) &= D_{NS}^h(m, q_0^2) \cdot a_m^{NS} \quad (\text{see equ. (19)}) \\ D_S^h(m, q^2) &= D_S^h(m, q_0^2) \cdot [a_m^+ + A_m (a_m^- - a_m^+)] \\ &\quad - D_G^h(m, q_0^2) \cdot 2fC_m [a_m^- - a_m^+] \end{aligned} \quad (25)$$

$$\text{with } a_m^i \equiv a_m^i(q^2, q_0^2) = \left(\frac{\ln \frac{q_0^2}{\Lambda^2}}{\ln \frac{q^2}{\Lambda^2}} \right)^{d_m^i} \quad (i=NS, +, -)$$

$$A_m = \frac{d_m^+ - d_m^{NS}}{d_m^+ - d_m^-}$$

$$C_m = \frac{d_m^{Gq}}{d_m^+ - d_m^-}$$

The d_m^i are the anomalous dimensions in the notation of ref. 36. $D_{NS}^h(m, q_0^2)$, $D_S^h(m, q_0^2)$ and $D_G^h(m, q_0^2)$ are the NS, S and gluon moments to be determined from experiment at some normalisation point $q^2 = q_0^2$. The gluon fragmentation function occurs due to the diagrams on the right-hand side in Fig. 20.

In the following we omit the indices h and m for simplicity. Defining

$$R(q^2) \equiv D_S(q^2)/D_{NS}(q^2) \quad (26)$$

as the ratio of S moment to NS moment one obtains from (25)³⁷:

$$\frac{R(q^2)}{R(q_0^2)} a^{NS} - a^+ = [A - P(q_0^2)C] \cdot (a^- - a^+) \quad (27)$$

where

$$P(q^2) \equiv 2fD_G(q^2)/D_S(q^2) \quad (28)$$

is the ratio of gluon moment to average-quark moment (remember that D_S is a sum over all quarks and antiquarks, see equ. (31)). For fixed q_0^2 equ. (27) is a straight line (going through the origin) of

$$\begin{aligned} y(q^2, q_0^2) &\equiv \frac{R(q^2)}{R(q_0^2)} a^{NS}(q^2, q_0^2) - a^+(q^2, q_0^2) \quad \text{vs} \\ x(q^2, q_0^2) &\equiv a^-(q^2, q_0^2) - a^+(q^2, q_0^2) \end{aligned} \quad (29)$$

with a slope of $A - P(q_0^2)C$ from which the ratio $P(q_0^2)$ at q_0^2 can be determined. Knowing from there $D_G(q_0^2)$ the QCD-predicted q^2 dependence of the gluon moments is then given by²⁸

$$\begin{aligned} D_G^h(m, q^2) &= D_G^h(m, q_0^2) [a_m^- + A_m (a_m^+ - a_m^-)] \\ &\quad + D_S^h(m, q_0^2) \cdot \frac{A_m (1 - A_m)}{2fC_m} [a_m^+ - a_m^-] \end{aligned} \quad (30)$$

Assuming the secondary hadrons to be pions and $h = \pi^+$ the ratio $R(q^2)$ can be determined in neutrino scattering from the measurable ratio $S(q^2) \equiv D_u^-(q^2)/D_u^+(q^2)$ of positive to negative moment:

$$\begin{aligned} D_{NS}^+ &= D_u^+ - D_u^- \quad (\text{see equ. (21)}) \\ D_S^+ &= D_u^+ + D_{\bar{u}}^+ + D_d^+ + D_{\bar{d}}^+ + D_s^+ + D_{\bar{s}}^+ \end{aligned} \quad (31)$$

Using charge-conjugation invariance and isospin symmetry one obtains for an SU(3)-symmetric sea ($f=3$, $D_{\bar{u}}^+ = D_d^+ = D_s^+ = D_{\bar{s}}^+ = D_u^-$, $D_{\bar{d}}^+ = D_u^-$)

$$D_S^+ = 2D_u^+ + 4D_u^- \quad \swarrow \quad R = 2 \frac{1+2S}{1-S} \quad (32)$$

For SU(2) symmetry ($f=2$, $D_{\bar{s}}^+ = D_s^+ = 0$) the relation is slightly different?

$$D_S^+ = 2D_u^+ + 2D_u^- \quad \swarrow \quad R = 2 \frac{1+S}{1-S} \quad (33)$$

Preliminary results on $P(q_0^2)$ have been obtained³⁷ from the data of the BEBC νH_2 experiment⁹. Fig. 31 shows for $f=2, m=2, q_0^2=10 \text{ GeV}^2$ and $\Lambda^2=0.65 \text{ GeV}^2$ the data points $y(q^2, q_0^2)$ plotted vs $x(q^2, q_0^2)$. As predicted they fall on a straight line with a slope which yields $P(m=2, q_0^2=10 \text{ GeV}^2) \approx 1$. Thus for $m=2$ the gluon-fragmentation moment is roughly equal to the average quark-fragmentation moment. This result is consistent with the energy-conservation sum rules:

$$\begin{aligned} \int_h D_G^h(m=2) &= \int_h z D_G^h(z) dz = 1 \\ \int_h D_S^h(m=2) &= \sum_{h, q, \bar{q}} \int_{q, \bar{q}} z D_q^h(z) dz = 2f \end{aligned} \quad (34)$$

if one assumes that in both cases $\sim \frac{2}{3}$ of the energy goes into charged hadrons.

In the same way the ratio $P(m, q_0^2)$ has been obtained for higher orders m as summarized in Fig. 32. It is seen that at $q_0^2=10 \text{ GeV}^2$ the gluon moments are ~ 1 to 1.5 times the average quark moments, which indicates that the quark

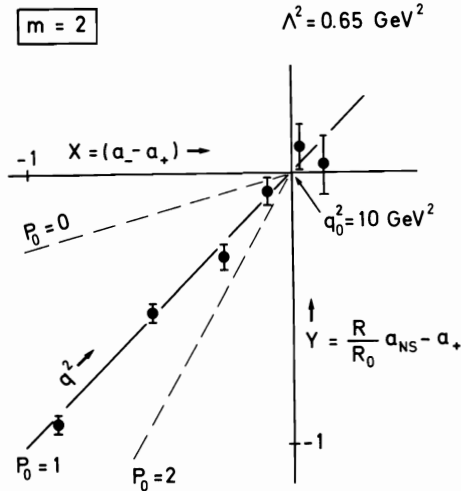


Fig. 31: Plot of $y(m, q^2, q_0^2)$ vs $x(m, q^2, q_0^2)$ (defined in the text, equ. (29)) for $m=2$, $f=2$, $q_0^2=10 \text{ GeV}^2$ and $\Lambda^2=0.65 \text{ GeV}^2$ from BEBC νH_2 ^{9,37}. The straight lines show the QCD prediction for $P(m, q_0^2) = 0, 1, 2$ (see equ. (27)) (preliminary).

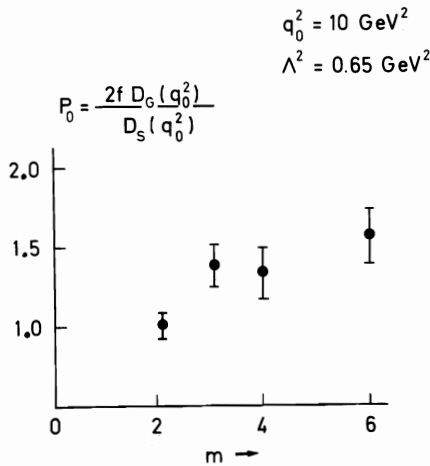


Fig. 32: The ratio $P_0 \equiv P(m, q_0^2) = 2f D_G(m, q_0^2) / D_S(m, q_0^2)$ vs. m for $f=2$, $q_0^2 = 10 \text{ GeV}^2$ and $\Lambda^2 = 0.65 \text{ GeV}^2$ from BEBC νH_2 ^{9,37} (preliminary).

and gluon fragmentation functions are rather similar.

C.) Transverse properties of single hadrons

In the simplest version of the naive QPM the fragmenting quark has no transverse momentum. This is changed in perturbative QCD where, due to gluon bremsstrahlung or quark-antiquark pair production from a gluon in the nucleon, the fragmenting parton (quark or gluon) acquires a transverse momentum k_T^{QCD} ³⁸.

The contributing diagrams are shown in Fig.33 taken from ref. 39. In addition there are two non-perturbative contributions: The original parton may have a primordial k_T^{prim} inside the nucleon ⁴⁰ and the hadron fragment gets a

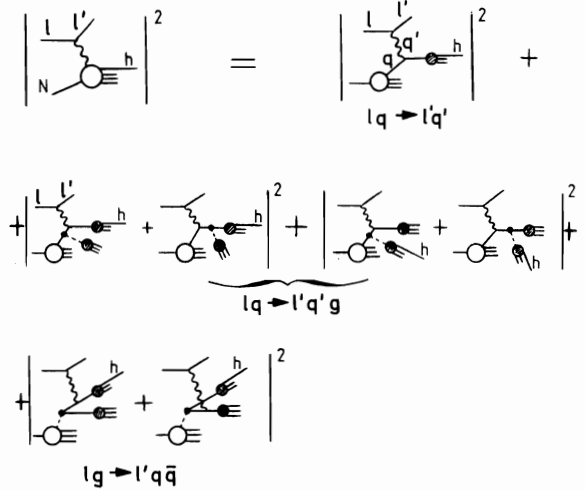


Fig. 33: The zeroth and first order QCD diagrams contributing to semi-inclusive neutrino production, from ref. 39.

k_T^{frag} with respect to the fragmenting parton from the fragmentation (hadronisation) process. The average p_T^2 of the observed hadron is thus composed of the three contributions in the following way ^{40,41}:

$$\langle p_T^2 \rangle = \left(\langle k_T^{2\text{prim}} \rangle + \langle k_T^{2\text{QCD}} \rangle \right) z^2 + \langle k_T^{2\text{frag}} \rangle \quad (35)$$

The factor z^2 occurs since only a fraction z of the parton momentum is transferred to the hadron. The dependences of the various contributions on the relevant variables (x, y, q^2, W) are discussed in the theoretical literature.

In particular QCD predicts ³⁸ for the QCD term at fixed x and y a q^2 dependence of the form

$$\langle k_T^{2\text{QCD}} \rangle \propto q^2 \alpha_s(q^2) \propto q^2 / \ln \frac{q^2}{\Lambda^2} \quad (36)$$

whereas the other contributions should not (strongly) depend on q^2 . However, the simple q^2 dependence in (36) is considerably distorted after integrating over x and y at fixed neutrino energy E_ν ^{38,42} and is more or less washed out when integrated over the spectrum of a wide or narrow band beam. On the other hand a strong W^2 dependence is predicted independent of E_ν . These theoretical q^2 and W^2 dependences are shown in Fig. 34 from ref. 42.

Altarelli ⁴³ predicts roughly

$$\langle k_T^{2\text{QCD}} \rangle \propto W^2 / \ln \frac{q^2}{\Lambda^2} \quad (37)$$

for all x .

Experimentally a problem arises in measuring p_T , since the current direction in the lepton plane is not well known due to the uncertainty in estimating the neutrino energy (see Introduction) ⁴⁴. Two methods have been used to overcome this difficulty:

- Instead of measuring p_T one measures $p_{T\text{out}}$, the component of p_T perpendicular to the well determined lepton plane (Fig.2). $p_{T\text{out}}$ is not affected by the uncertainty inside the lepton plane. Assuming azimuthal isotropy in φ , $\langle p_{T\text{out}}^2 \rangle = \frac{1}{2} \langle p_T^2 \rangle$.
- One measures p_T not with respect to the current direction (=direction of the system of all hadrons) but with respect to the momentum of all charged hadrons assuming that the systems of neutral particles and of charged particles have nearly the same direction. Since this is only approximately true this $\langle p_T \rangle$ could be smaller than the genuine $\langle p_T \rangle$.

From previous experiments^{4-7,44} the following results have been obtained:

- The p_T^2 distributions $d\sigma/dp_T^2$ can well be fitted by e^{-Bm_T} (where m_T is the transverse mass and $B \approx 6 \text{ GeV}^{-1}$) and are not so well described by a Gaussian in p_T^2 .
- $\langle p_T \rangle$ increases with increasing x_F or z (seagull effect).
- In νN scattering $\langle p_T^2 \rangle$ increases at high E_ν with q^2 , in particular for $z \gtrsim 0.2$. In $\bar{\nu} N$ scattering (and in νN at lower E_ν) no such increase is observed. These two results are not inconsistent with each other, since at fixed q^2 the average W is lower in $\bar{\nu} N$ than

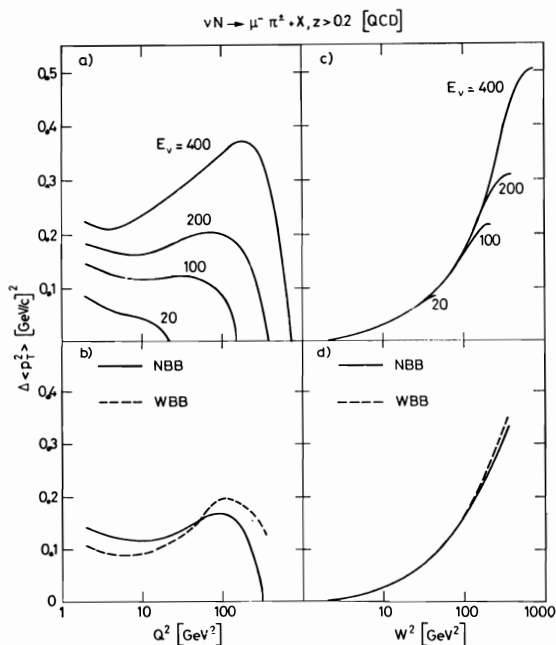


Fig. 34: QCD predictions of $\langle p_T^2 \rangle$ of secondary hadrons with $z > 0.2$ from neutrino production vs q^2 (a,b) and vs W^2 (c,d) for fixed neutrino energies (a,c) and for wide and narrow band beams (b,d), from ref. 42.

in νN due to the lower $\bar{\nu}$ energy spectrum and the suppression of larger y values by the $(1-y)^2$ distribution ($W^2 = M^2 + 2ME_\nu y - q^2$).

- $\langle p_T^2 \rangle$ increases with W^2 in νN , whereas in $\bar{\nu} N$ the situation is not clear yet because of larger statistical errors.

Fig. 35 shows a new measurement of the p_T^2 distribution of charged hadrons in νp and νn reactions by the 15' νD_2 collaboration²³. It is seen that the distribution is the same for νp and νn and that an exponential in m_T gives a better fit to the data than an exponential in p_T^2 .

New (preliminary) results on $\langle p_T^2 \rangle$ have been obtained by the BEBC νH_2 collaboration⁹. Fig. 36 shows $\langle p_T^2 \rangle$ (with respect to the current and charged-hadron direction) and $\langle p_{T\text{out}}^2 \rangle$ of charged hadrons with $x_F > 0$ vs q^2 and W^2 for all z and for three different intervals of z . The following conclusions can be drawn from the figure:

- The corresponding $\langle p_T^2 \rangle$ values with respect to the current direction and to the charged-hadron direction are in good agreement with each other so that the uncertainty from estimating the neutrino energy has no noticeable influence. Furthermore $\langle p_{T\text{out}}^2 \rangle \approx \frac{1}{2} \langle p_T^2 \rangle$ as expected.
- $\langle p_T^2 \rangle$ increases with z (seagull effect). A

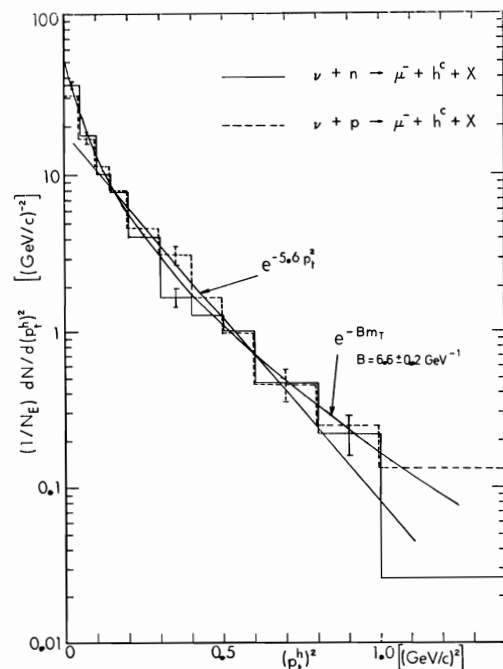


Fig. 35: p_T^2 distribution of charged hadrons in νp and νn reactions from 15' νD_2 ²³.

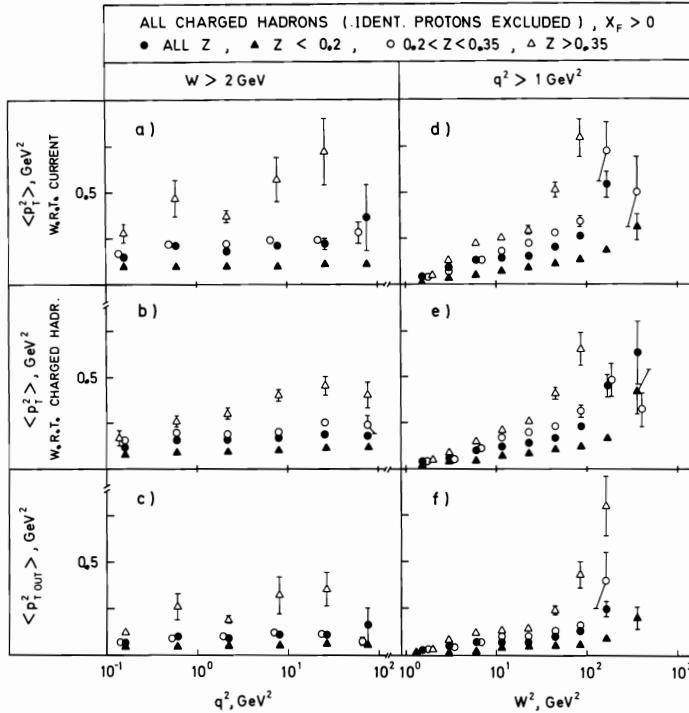


Fig. 36: (a,d) $\langle p_T^2 \rangle$ with respect to current direction, (b,e) $\langle p_T^2 \rangle$ with respect to charged-hadron direction and (c,f) $\langle p_{T\text{out}}^2 \rangle$ of single forward going ($x_F > 0$) charged hadrons for all z and three different z intervals vs q^2 (a,b, c) and W^2 (d,e,f) from BEBC νH_2 ⁹ (preliminary).

statistically significant q^2 dependence is observed only for the highest z range ($z > 0.35$) in Fig. 36b. The W^2 dependence on the other hand is much stronger; $\langle p_T^2 \rangle$ increases with increasing W^2 , the increase being the stronger the higher z is.

- Both q^2 and W^2 dependences are in qualitative agreement with the dependences predicted by QCD in Fig. 34. Quantitatively however there are discrepancies, the experimental values tending to be larger than the QCD predicted ones. This is probably due to contributions from a primordial k_T and fragmentation k_T , equ. (35), as pointed out also in ref. 42. It is however difficult to disentangle the three contributions in equ. (35) experimentally from the data in Fig. 36.

Positive and negative hadrons turned out to have the same $\langle p_T^2 \rangle$ within the statistical errors.

In analogy to the moments of the distribution in the longitudinal variable z , the moments of the distribution of the scaled transverse momentum $x_T = 2p_T/W$ (or $x_{T\text{out}} = 2p_{T\text{out}}/W$) have been determined by the BEBC $\nu\text{Ne-H}_2$ ⁴⁵ and BEBC νH_2 ⁹ collaborations:

$$D_T^\pm(m, q^2) = \frac{1}{N_{\text{ev}}} \int_0^{x_T} x_T^{m-1} \frac{dN^\pm}{dx_T} dx_T \quad \text{or} \quad (38)$$

$$D_{T\text{out}}^\pm(m, q^2) = \frac{1}{N_{\text{ev}}} \int_0^{x_{T\text{out}}} x_{T\text{out}}^{m-1} \frac{dN^\pm}{dx_{T\text{out}}} dx_{T\text{out}}$$

Fig. 37 shows the non-singlet moments $D_T^{\text{NS}} = D_T^+ - D_T^-$ of orders $m = 2, 3, 4$ vs q^2 and W^2 for Bjorken $x < 0.2$ (open symbols) and $x > 0.2$ (full symbols) from ref. 45. The moments depend strongly on q^2 and W^2 . The interesting feature to be observed is the fact that the moments depend also on x at fixed q^2 whereas they are independent of x at fixed W . The same behavior is observed for the non-singlet $x_{T\text{out}}$ moments from BEBC νH_2 ⁹, shown in Fig. 38. This implies factorisation (non-factorisation) in x and x_T at fixed W (fixed q^2) similar to the result obtained for the moments of the z distributions as discussed above.

D.) Jet Studies

The quantities sphericity S , sphericity S' and thrust T are used to investigate the jet properties of e^+e^- annihilation or leptoproduction events. S , S' and T are defined as⁴⁶⁻⁴⁹

$$S = \left(\frac{4}{\pi}\right)^2 \min \left(\frac{\sum p_{Ti}}{\sum p_i} \right)^2$$

$$S' = \frac{3}{2} \min \frac{\sum p_{Ti}^2}{\sum p_i^2} \quad (39)$$

$$T = 2 \max \frac{\tilde{\sum p_{Li}}}{\sum p_i}$$

where the sums Σ and $\tilde{\Sigma}$ extend over all final state particles and over those in one hemi-

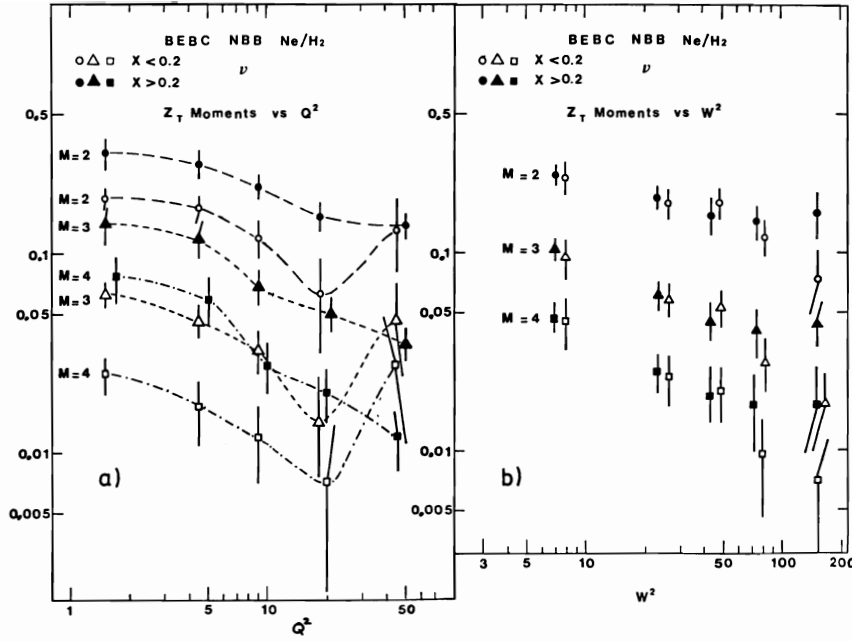


Fig. 37: Non-singlet moments D_T^{NS} ($m=2,3,4$) of the distributions in $x_T = 2p_T/W$ of hadrons (all x_F) vs (a) q^2 and (b) W^2 for Bjorken $x < 0.2$ (open symbols) and $x > 0.2$ (full symbols). The curves are to guide the eye. From BEBC ν Ne- H_2 ⁴⁵ (preliminary).

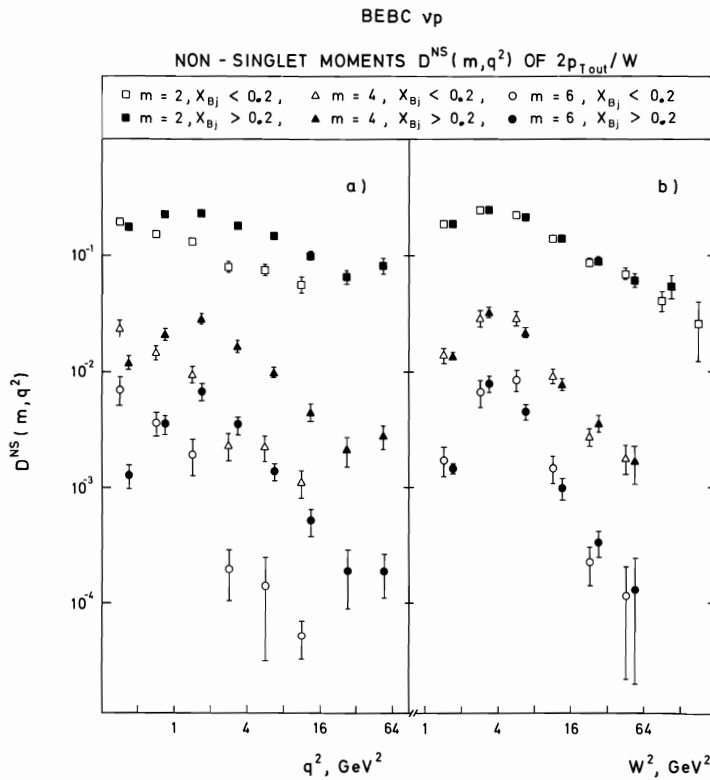


Fig. 38: Non-singlet moments D_{Tout}^{NS} ($m=2,4,6$) of the distributions in $x_{Tout} = 2p_{Tout}/W$ of hadrons with $x_F > 0$ vs (a) q^2 and (b) W^2 for Bjorken $x < 0.2$ (open symbols) and $x > 0.2$ (full symbols) from BEBC νH_2 ⁹ (preliminary).

sphere, respectively. p_{Ti} and p_{Li} are the transverse and longitudinal momenta of the i th particle in the hadronic cm system with respect to axes which respectively minimize S , S' or maximize T . In leptonproduction these two axes nearly coincide with the current direction \vec{q} at high W ⁵⁰.

For neutrino production, the predictions of

the naive QPM (0th order QCD) and of 1st order QCD for the S and T distributions at fixed W and for the averages $\langle S \rangle$ and $\langle 1-T \rangle$ as functions of W have been calculated by Binétruy and Girardi⁵¹ and by Ranft and Ranft⁵²:

a.) The naive QPM yields a final state of a forward going quark q and a backward going diquark qq which go back-to-back to each other if one neglects the primordial

k_T . On the parton level (i.e. neglecting hadronisation and taking the momenta of the partons or of their respective jets as a whole) one thus obtains $T=1$ and $S=S'=0$. These δ -function-like distributions are smeared out if one includes the non-perturbative hadronisation of quarks into hadrons with a finite k_T of hadrons with respect to the quark direction ("Fragmentation jets"⁵³). In this case the forward (q) and backward (qq) jets should be similar in size.

- b.) In 1st order QCD one obtains three partons (or parton jets) in the final state, namely diquark-quark-gluon (by gluon bremsstrahlung) or triquark-quark-antiquark (by $q\bar{q}$ pair production), see Fig. 33 ("QCD jets"⁵³). The resulting S and T distributions are then smeared out due to hadronisation. In this case the forward (qq or $q\bar{q}$) jet should be wider than the backward jet.

The predicted differential cross sections in T, normalized to the zeroth order inclusive cross section, are shown in Fig. 39 for $W=6, 10$ and 14 GeV. It is seen that the non-perturbative (NP) zeroth-order cross section clearly dominates over the 1st order-QCD cross section even if one includes hadronisation in the latter (dashed curves). Only at $W \gtrsim 20$ GeV (where practically no data are available) does the QCD cross section begin to dominate for $T \lesssim 0.8$.

Included in Fig. 39 are preliminary data points⁵⁴ obtained by the BEBC ν Ne-H₂ collaboration for $W > 6$ GeV. They are in rough agreement with the NP prediction and demonstrate that at presently available W values it is not yet possible to observe any hard QCD effects; they are hidden by the non-perturbative

effects. The same conclusion is obtained in a recent publication⁵⁵ of the same collaboration. Fig. 40 shows the normalized S and T distributions for $8 < W < 12$ GeV and Fig. 41 the average values $\langle S \rangle$ and $\langle 1-T \rangle$ vs W together with results from e^+e^- annihilation and π^- Ne scattering. The results in Fig. 41 from the various reactions are in surprising agreement with each other and cannot be accounted for by 1st order QCD (solid line for νN ⁵¹, dashed line for e^+e^- ⁴⁶). Assuming the parton picture, it is the non-perturbative hadronisation process described under a.) above and not a QCD process (bremsstrahlung or pair production) which determines the S and T distributions at present W values. It was found furthermore that $\langle S \rangle$ and $\langle 1-T \rangle$ do not depend on Bjorken x at fixed W.

New results on sphericity S' and thrust T have also been submitted to this conference by the 15' $\bar{\nu}H_2$ collaboration⁵⁰. Figs. 42a and b show the averages $1-\langle T \rangle$ and $\langle S' \rangle$ respectively vs W for $\bar{\nu}p$ and νp reactions and for e^+e^- annihilation. The results on $\langle T \rangle$ are in good agreement with the data in Fig. 41b. Fig. 43 shows the normalized sphericity distribution for neutrino production and e^+e^- annihilation for two regions of W. In both Figs. 42 and 43 again good agreement between the results for neutrino production and e^+e^- annihilation is observed indicating that for $W \gtrsim 15$ GeV the two types of reactions exhibit very similar jet properties. This is in accord with the expectation from non-perturbative hadronisation in the naive QPM whereas hard gluon effects according to QCD would lead to differences in neutrino production and e^+e^- annihilation (see e.g. curves in Fig. 41b). Indeed the recent PETRA results show that the emission of hard gluons is observable only at much higher energies ($W \gtrsim 30$ GeV).

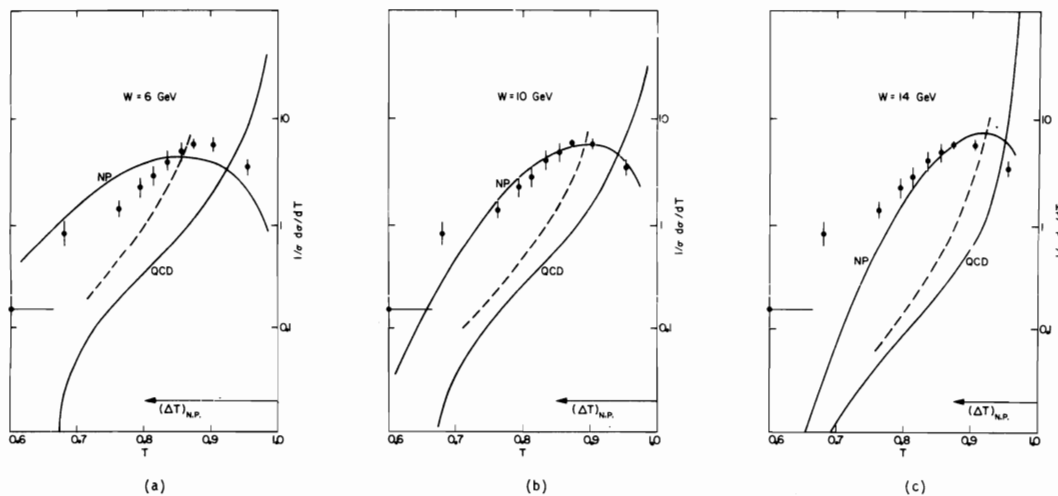


Fig. 39: Predictions of 1st order QCD without (full curves) and with (dashed curves) hadronisation and of the naive quark parton model with non-perturbative (NP) hadronisation for the normalized differential cross section in thrust T for $q^2 > 1$ GeV² and 3 values of W in neutrino production, from ref. 51. The data points are preliminary results from BEBC ν Ne-H₂⁵⁴ for $W > 6$ GeV.

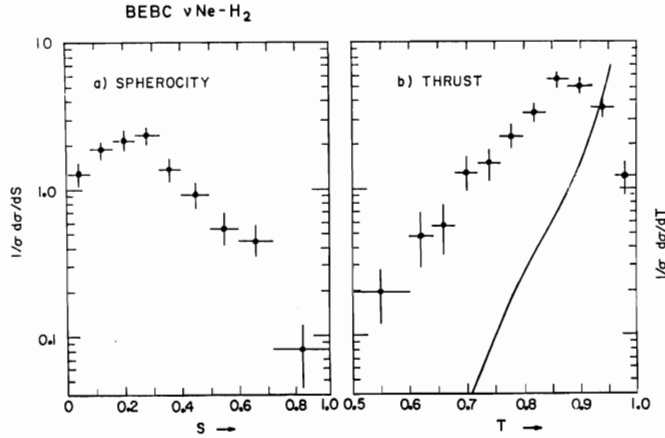


Fig. 40: Normalized (a) sphericity distribution and (b) thrust distribution from BEBC $\nu\text{Ne-H}_2$ ⁵⁵ for $8 < W < 12$ GeV. The curve shows the prediction of 1st order QCD without hadronisation.

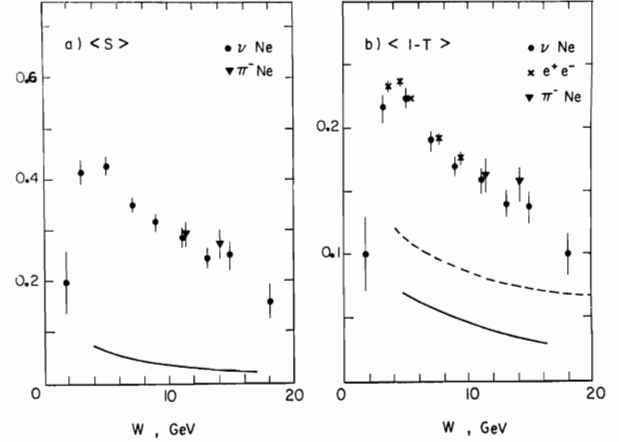


Fig. 41: Average values of (a) sphericity and (b) thrust vs W for neutrino and π^- reactions in Ne-H_2 from BEBC $\nu\text{Ne-H}_2$ ⁵⁵ and for e^+e^- annihilation. The curves show the predictions of 1st order QCD for neutrino production (full curves) and e^+e^- annihilation (dashed curve).

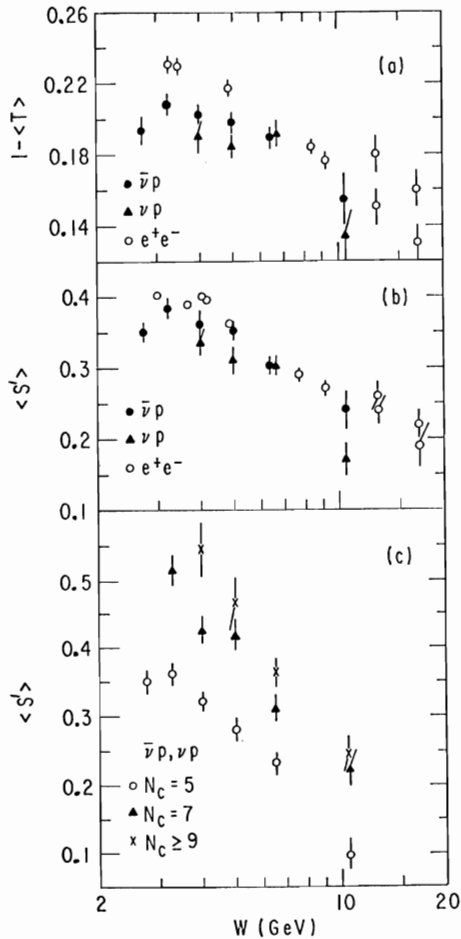


Fig. 42: Average (a) thrust and (b) sphericity vs W for $\bar{\nu}p$ and νp reactions and for e^+e^- annihilation; (c) average sphericity vs W for fixed charged multiplicity in $\bar{\nu}p$ plus νp reactions. From 15' $\bar{\nu}\text{H}_2$ ⁵⁰.

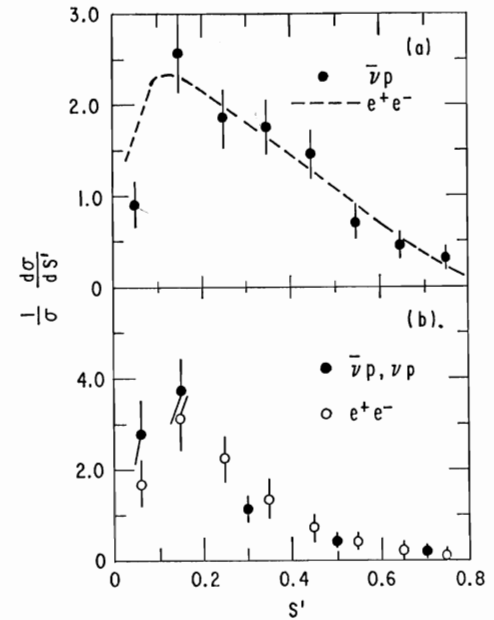


Fig. 43: (a) normalized sphericity distribution for $\bar{\nu}p$ reactions with $\langle W \rangle = 6.6$ GeV (points) and for e^+e^- annihilation at $W = 7$ GeV (curve). (b) normalized sphericity distribution for $\bar{\nu}p$ plus νp reactions with $\langle W \rangle = 10.5$ GeV (full points) and for e^+e^- annihilation at $W = 13$ GeV (open points). From 15' $\bar{\nu}\text{H}_2$ ⁵⁰.

Finally, the angular distributions of energy flow into the forward and backward hemispheres in $\bar{\nu}p$ interactions, shown in Fig. 44, indicate that the forward and backward jets have very similar shape. This again is predicted by the naive QPM with hadronisation (see above).

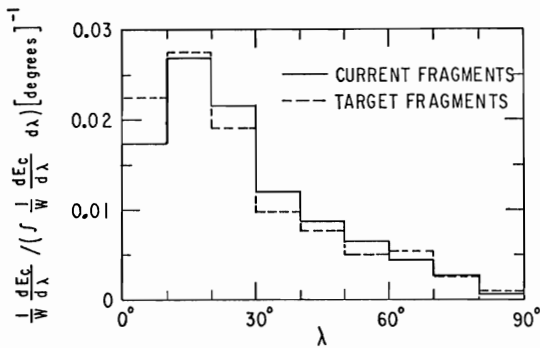


Fig. 44: Angular distribution of energy flow with respect to the thrust axis for $\bar{\nu}p$ interactions with $W > 4.5$ GeV and thrust $T > 0.85$. The solid (dashed) histogram is for hadrons going into the forward (backward) hemisphere defined by a plane perpendicular to the thrust axis. From 15' $\bar{\nu}H_2$ 50'.

Summary

This summary gives a list of what I think are the most interesting new experimental results on hadronic final states produced in charged current neutrino and antineutrino reactions:

- The multiplicity distribution obeys KNO scaling with a scaling curve which is in good agreement with that measured for $p\bar{p}$ annihilation.
- The charge distributions in νN and $\bar{\nu} N$ scattering at high W show a clear step at $y^* = 0$ in the cm system.
- The total net charges of forward going hadrons are in good agreement with the naive QPM.
- The fragmentation functions show non-scaling if all W values are included. For the non-singlet combination, the observed scaling violation is in surprising agreement with 1st order QCD.
- The semi-inclusive cross section does not factorize in x and z at fixed (low) q^2 , whereas it seems to factorize at fixed W .
- At $q_0^2 = 10$ GeV² the gluon moments are roughly equal to the average quark moments.
- $\langle p_T^2 \rangle$ depends little on q^2 , but strongly on W^2 . Although these dependences are predicted by 1st order QCD there is no quantitative agreement, and non-perturbative effects contribute considerably.
- There is non-factorisation in x and x_T at fixed q^2 , whereas factorisation is observed at fixed W .
- At present W values ($W \lesssim 15$ GeV) the jet properties of neutrino production events are determined by non-perturbative hadronisation and not by hard gluon effects.
- The jet properties of neutrino production events are very similar to those of e^+e^- annihilation for $W \lesssim 15$ GeV.

It is a great pleasure to thank my colleague W. Wittek for his permanent and invaluable help during the preparation of this report. He has made essential contributions, in particular by many fruitful discussions, by preparing the figures and by his critical reading of the manuscript. I express my gratitude to my secretary E. Thurner for her patient and diligent work in typing the manuscript and in arranging the figures in the text. I am grateful to Fermilab for their hospitality and manifold support extended to me before and during the conference, and in particular to J. Feller for his valuable assistance as a Scientific Secretary. Finally I would like to thank my colleagues in the various collaborations for many enlightening discussions.

References

- 1.) G. Myatt: CERN ECFA Report 72/4, Vol. 2, 117 (1972)
- 2.) A. Grant: Nucl.Inst.Meth. 127, 355 (1975)
- 3.) H.G. Heilmann: Bonn Internal Report WA21-int-1 (1978)
- 4.) M. Derrick et al.: Phys.Rev. D17, 1 (1978)
- 5.) J.P. Berge et al.: Phys.Rev. D18, 3905 (1978); V. Ammosov et al.: Nuov.Cim. 51A, 539 (1979)
- 6.) J. Bell et al.: Phys.Rev. D19, 1 (1979)
- 7.) P.C. Bosetti et al.: Nucl.Phys. B149, 13 (1979)
- 8.) R.D. Field, R.P. Feynman: Nucl.Phys. B136, 1 (1978)
- 9.) Aachen-Bonn-CERN-München-Oxford collaboration ($\bar{\nu}H_2$ in BEBC)
- 10.) C.K. Chen et al.: Nucl.Phys. B133, 13 (1978)
- 11.) J. Ballam et al.: Phys.Lett. 56B, 193 (1975)
- 12.) H.H. Bingham et al.: Phys.Rev. D8, 1277 (1973)
- 13.) Z. Koba, H.B. Nielsen, P. Olesen: Nucl. Phys. B40, 317 (1972)
- 14.) D.R.O. Morrison: Proc. 19th Intern.Conf. on High Energy Physics, Tokyo, p. 354 (1978)
- 15.) B. Musgrave (Argonne, Carnegie-Mellon, Purdue Collaboration, $\bar{\nu}H_2$ in 15'): paper submitted to the Neutrino 79 Conf. at Bergen, Norway (1979), and to this conference; M. Derrick et al.: paper submitted to this conference (preprint no. ANL-HEP-CP-79-21)
- 16.) K.H. Streng, T.F. Walsh, P.M. Zerwas: DESY 79/10 (1979), Z. Physik C
- 17.) J.D. Bjorken: Int. Summer Inst.on Theor. Part.Phys., J.G. Körner et al. Editors, p. 93 (1975)
- 18.) G.R. Farrar, J.L. Rosner: Phys.Rev. D7, 2747 (1973); R.N. Cahn, E.W. Colglazier: Phys. Rev. D9, 2658 (1974); J.L. Newmeyer, D. Sivers: Phys.Rev. D9, 2592 (1974); S.J. Brodsky, N. Weiss: Phys.Rev. D16, 2325 (1977)
- 19.) S.L. Glashow: remark made at the Neutrino 79 Conf. at Bergen, Norway (1979)

- 20.) J.P. Berge et al. (Fermilab, IHEP, ITEP, Michigan collaboration, $\bar{\nu}\text{Ne-H}_2$ in 15'): paper submitted to the Neutrino 79 Conf. at Bergen, Norway (1979)
- 21.) W.G. Scott: Physica Scripta 19, 179 (1979)
- 22.) H.J. Lubatti (Berkeley, Hawaii, Seattle collaboration, $\nu, \bar{\nu}\text{Ne-H}_2$ in 15'): paper submitted to the Neutrino 79 Conf. at Bergen, Norway (1979)
- 23.) T. Kafka et al. (Illinois-Tech, Maryland, Sendai, Stony Brook, Tufts collaboration, νD_2 in 15'): paper submitted to this conference
- 24.) Y.G. Rjabov (IHEP, $\nu\text{CF}_3\text{Br}$ in SKAT): paper submitted to this conference
- 25.) R.P. Feynman: Photon-Hadron Interactions, Benjamin, Reading/Mass. (1972)
- 26.) R.D. Field, R.P. Feynman: Phys.Rev. D15, 2590 (1977)
- 27.) L.M. Sehgal: Proc. 1977 Intern.Symp. on Lepton and Photon Int. at High Energies at Hamburg, p. 837 (1977)
- 28.) J.F. Owens: Phys.Lett. 76B, 85 (1978)
T. Uematsu: Phys.Lett. 79B, 97 (1978)
- 29.) G. Altarelli, G. Parisi: Nucl.Phys. B126, 298 (1977)
- 30.) N. Sakai: Phys.Lett. 85B, 67 (1979)
- 31.) G. Altarelli, R.K. Ellis, G. Martinelli, So-Young Pi: preprint CTP no. 793, submitted to Nucl.Phys. (1979)
- 32.) R. Baier, K. Fey: Bielefeld-preprint BI-TP 79/11 (1979)
- 33.) J. Blietschau et al.: paper submitted to Phys.Lett., contributions to the Neutrino 79 Conf. at Bergen, Norway, and to the EPS Intern.Conf. on High Energy Physics, Geneva (1979)
- 34.) W.G. Scott (Aachen, Bonn, CERN, Munich, Oxford collaboration); paper presented at 7. Intern. Winter Meeting on Fundamental Physics, Segovia, Spain (1979)
- 35.) J. Ellis, M.K. Gaillard, W.J. Zakrzewski: Phys.Lett. 81B, 224 (1979)
- 36.) I. Hinchliffe, C.H. Llewellyn Smith: Nucl.Phys. B128, 93 (1977)
- 37.) D.H. Perkins; private communication and Rapporteur's talk at the Neutrino 79 Conf. at Bergen, Norway (1979)
- 38.) A. Mendez: Nucl.Phys. B145, 199 (1978); G. Altarelli, G. Martinelli: Phys.Lett. 76B, 89 (1978); A. Mendez, A. Raychaudhuri, V.J. Stenger: Nucl.Phys. B148, 499 (1979)
- 39.) A. Mendez: Proc.Top.Conf. on Neutrino Phys. at Accel., Oxford, p. 131 (1978)
- 40.) M. Glück, E. Reya: Nucl.Phys. B145, 24 (1978)
- 41.) M. Gronau, Y. Zarmi: Phys.Rev. D18, 2341 (1978)
- 42.) P. Mazzanti, R. Odorico, V. Roberto: Phys.Lett. 81B, 219 (1979)
- 43.) G. Altarelli: Proc. 13th Rencontre de Moriond, Vol.II, p. 395 (1978)
- 44.) V.J. Stenger: Proc.Top.Conf. on Neutrino Phys. at Accel., Oxford, p. 99 (1978)
- 45.) B. Tallini: Rapporteur's talk at the EPS Intern.Conf. on High Energy Physics, Geneva (1979)
- 46.) A. De Rujula, J. Ellis, E.G. Floratos, M.K. Gaillard: Nucl.Phys. B138, 387 (1978)
- 47.) H. Georgi, M. Machacek: Phys.Rev.Lett. 39, 1237 (1977)
- 48.) J.D. Bjorken, S.J. Brodsky: Phys.Rev. D1, 1416 (1970)
- 49.) E. Farhi: Phys.Rev.Lett. 39, 1587 (1977)
- 50.) M. Derrick et al. (Argonne, Carnegie-Mellon, Purdue collaboration, $\bar{\nu}\text{H}_2$ in 15'): paper submitted to this conference (preprint no. ANL-HEP-PR-79-17)
- 51.) P. Binétruy, G. Girardi: Nucl.Phys. B155, 150 (1979)
- 52.) J. Ranft, G. Ranft: Phys.Lett. 82B, 129 (1979)
- 53.) P.M. Stevenson: Nucl.Phys. B150, 357 (1979); B156, 43 (1979)
- 54.) A. Vayaki: Proc.Top.Conf. on Neutrino Phys. at Accel., Oxford, p. 46 (1978)
- 55.) K.W.J. Barnham et al.: Phys.Lett. 85B, 300 (1979)

Discussion

Derrick, Argonne:

We know that heavy charmed particle production is large in νN collisions and that the z distribution is flatter for the heavier particles than for pions. The observation of an increase in $\langle p_T \rangle$ with W at high z may come from this effect. Do you know of any quantitative estimation of this contribution?

Schmitz:

No, I don't. However I am not sure if the charmed particle production is really large enough to produce the observed strong W dependence of $\langle p_T^2 \rangle$. It should be remembered that

neutral strange particles (possibly from charmed particle decay) were not included in the plot that I have shown.

Messing, Cornell:

The types of violations of the simple fragmentation model that you have discussed and attributed possibly to QCD, were seen in electroproduction data presented two years ago by L. Hand at the Hamburg conference. Using other narrow spectrometer data one could show that all those violations were essentially due to proton production. If you compare the electroproduction data with neutrino data you can get a similar prediction. In fact 30% of the positive hadrons that you are plotting in your distribution are protons. Since all the predictions are for pions how can you justify even discussing QCD?

Schmitz:

I cannot quite agree to your statements. First, a large fraction of the protons are identified in the bubble chamber pictures by ionisation, range, or energy loss. These identified protons have a z distribution with an accumulation at small z from protons going

backward in the cms, and an accumulation at large z from protons from Δ^{++} decay. Both accumulations are practically removed by the cuts applied in the analysis: the first by taking $x_F > 0$, the second by taking $q^2 > 1 \text{ GeV}^2$. The remaining unidentified protons are estimated to be less than 10% of all positive tracks. Secondly, these unidentified protons (treated as pions) enter with small z values, if they are target fragments. Small z values do however not contribute noticeably to the moments of higher order m . Thirdly, I have shown that the current fragments need not to be pions; the difference between particle and antiparticle moment is a non-singlet irrespective of the nature of the particle.

Heusch, Santa Cruz:

Is there any news about the q^2 dependence (at fixed W) of the topological cross sections? You may recall that low-energy νN and μN data had a flat q^2 behaviour which was difficult to build up out of individually identified channel cross sections.

Schmitz:

No, there are no new results that I know of. Of course the q^2 dependence of topological cross sections can easily be obtained from the data available from the various groups.

Wolf, DESY:

Do the data permit to say anything about the Fermi-momentum distribution of the quarks in the incoming nucleon?

Schmitz:

As I said, it has not yet been possible so far to disentangle cleanly the average primordial p_T of the parton inside the nucleon from the measured $\langle p_T \rangle$ of the final-state hadrons. It is certainly even much more difficult to determine a momentum distribution inside the nucleon; no results have been obtained so far.

Bialas, Cracow:

I don't have a question, I have a comment. I concluded for myself from the two last talks that it is time to stop calling the good old quark model the "naive" quark-parton model. It apparently fits the data very well. It may not be exactly correct, but it is certainly not naive. This is like calling Newtonian dynamics "naive". If this comment could be included in the proceedings I would be very happy.

Osborne, MIT:

You had a very dramatic difference between the data and the QCD predictions of sphericity, spherocity or thrust in a plot where you compare the naive (pardon me) quark-parton model and 1st order QCD. In fact, your error bars were so small compared to the difference between those predictions, that you could cut on much higher W and see if the same difference occurs there. In this way you could have a W comparable with that in recent e^+e^- experiments. Could you comment on that?

Schmitz:

Yes. The average values of thrust and sphericity/spherocity vs W which I showed you extended already to the highest available W values where any reasonable statistics are left. As one sees from the W distributions

e.g. in the 15' $\bar{\nu}H_2$ and BEBC νH_2 experiments, above $\sim 15 \text{ GeV}$ practically no events are left.